Journal of
Water & Climate Change

IWA PUBLISHING

Integrated flood risk assessment of the Arial Khan River under changing climate using IPCC AR5 risk framework

Binata Roy [iD][a], Md. Sabbir Mostafa Khan[b], A. K. M. Saiful Islam [iD][a,*], Md. Jamal Uddin Khan [iD][a] and Khaled Mohammed[a]

[a] Institute of Water and Flood Management (IWFM), Bangladesh University of Engineering and Technology (BUET), Dhaka 1000, Bangladesh
[b] Department of Water Resources Engineering, Bangladesh University of Engineering and Technology (BUET), Dhaka 1000, Bangladesh
*Corresponding author. E-mail: saiful3@gmail.com

[iD] BR, 0000-0002-2726-3340; AKMSI, 0000-0002-2435-8280; MJUK, 0000-0002-3494-4179

ABSTRACT

Bangladesh is situated at the confluence of GBM basins, with 90% of the basin area locating outside the country. Future climate change will lead to intense, prolonged, and frequent floods in Bangladesh. An integrated flood risk assessment that transforms flood risks from transboundary river basins to the local administrative level is necessary. A 1D/2D hydrodynamic model is developed for flood vulnerable Arial Khan River feed by basin-scale hydrologic model for low (RCP2.6) and high (RCP8.5) climate scenarios. An increasing trend in flood depth, duration, and area is observed from the early (2020s) to the end (2080s) of the century for both scenarios. The difference between both RCPs is minimal from the 2020s to 2050s but becomes very pronounced in the 2080s. The depth-duration-area with equal weightage provides better hazard results for the area. Flood risk is assessed using the IPCC AR5 framework incorporating vulnerability and exposure. Some medium-hazard zones fall into high-risk zones due to high exposure and vulnerability to flooding. The areas along the left reach are found more hazard-prone, while the areas on the right side are more risk-prone in the 2080s of RCP8.5. The hazard/risk maps will help policymakers identify priority areas for planning a sustainable flood management strategy.

Key words: AR5 risk framework, climate change, exposure, flood risk, hazard, vulnerability

HIGHLIGHTS

- Flood risk is transferred from transboundary river basins to local administrative levels using a multi-model hydrological-hydrodynamic-statistical modelling system.
- High-resolution bias-corrected GCM climate data is used.
- IPCC AR5 climate scenarios and risk framework are considered.
- Future flood hazard and risks are assessed for Arial Khan River Floodplain for the 2020s, 2050s, and 2080s.
- Medium hazard zones might have high flood risk in the future.

GRAPHICAL ABSTRACT
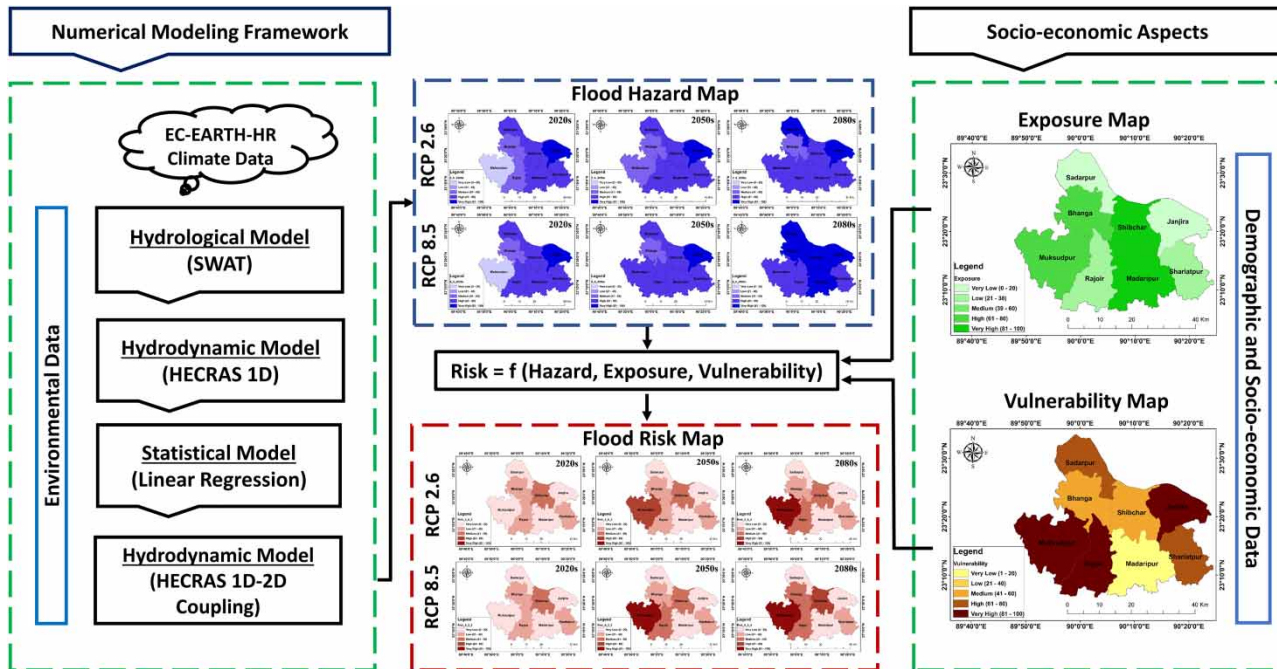
Arial Khan River Flood Hazard and Risk Maps using IPCC AR5 Risk Framework for RCP Climate Scenarios

1. INTRODUCTION

Bangladesh is highly susceptible to floods due to its location at the confluence of the world's three major basins – Ganges-Brahmaputra-Meghna (GBM) and hydro-meteorological and topographical characteristics of the basins (Shaw et al. 2013). About 92.5% of the combined basin lies outside of Bangladesh in the neighbouring countries: India, China, Nepal, and Bhutan (Mirza et al. 2003). Furthermore, about 80% of the annual rainfall occurs in the monsoon (June to September) across these river basins. Therefore, Bangladesh drains out huge cross-border runoff and internal runoff through a network of rivers moving towards the final destination – the Bay of Bengal. The volume of generated runoff exceeds the natural drainage capacity most of the time and causes frequent floods in Bangladesh.

On average, annual floods inundate 20% of the country, reaching as high as about 70% during extreme flood events (Mirza 2002). Increasing GHG emissions, global warming, and climate change will undoubtedly worsen the situation manifold. IPCC (International Panel on Climate Change) fifth assessment report (AR5) projects an increase in global temperature in between 0.3 and 4.8 °C for low (RCP – Representative Concentration Pathway 2.6) to high (RCP8.5) emission scenario by the end of 21st century (IPCC 2013). At the same time, the equatorial Pacific is likely to experience an increase in mean precipitation under the RCP8.5 scenario (IPCC 2013). Climate variability is also a factor in understanding the hydrologic cycle response due to global warming. Though changes in mean precipitation and temperature have been studied intensively in recent years, precipitation variability has gained less attention. However, the detection of spatial and temporal patterns of climate variability is a challenging issue. One of the most critical factors in choosing the time resolution which can result in different spatial and temporal patterns (Amiri & Mesgari 2017, 2019; Amiri et al. 2017). Higher inter-annual climate variability is reported to be increased in the future due to global warming (Pendergrass et al. 2017). Specifically, precipitation variability will increase 3–4% K^{-1} globally, and 4–5% K^{-1} over land and 2–4% K^{-1} over the ocean by the end of the 21st century under RCP8.5 (Pendergrass et al. 2017). All these projections indicate a significant change in the hydrological cycle of the GBM basins. Particularly, glaciers melting in the upper Hindu-Kush Himalayan (HKH) region will increase the flow in the GBM rivers, enhancing the risk of monsoon floods in Bangladesh. Simultaneously, the monsoon regime will increase precipitation in some of the places in Bangladesh. As a result, the frequency, intensity, and longevity of

floods will increase significantly in the future decades (Mohammed *et al.* 2018). Hence, a sustainable flood management plan considering climate change impact is necessary for Bangladesh.

At present, flood risk assessment is recognized as an essential input for formulating flood management plans and policies at the national, regional, and local levels (ISRBC 2014). Flood hazard and risk studies help planners and policymakers in identifying the priority areas for planning any future flood management strategies. Basin-scale assessment of climate change impact plays a vital role in this regard. It's crucial for Bangladesh since more than 90% of the upstream catchment area of the river systems of Bangladesh is located outside the country (Mirza *et al.* 2003). Ignoring the impact of the huge flow from upstream basins might result in inaccurate flood assessment. Hence, the transformation of floods from the basin scale to the local scale is inevitable and challenging. Regional-scale hydrologic modelling coupled with local-scale hydrodynamic modelling is a novel approach for incorporating the upstream basin flow inputs in local-scale flood hazard and risk assessment. Worldwide many such studies have been conducted so far. Dankers & Feyen (2008) studied the climate change impact in future floods in Europe using regional climate model HIRHAM and flood model LISFLOOD under IPCC Special Report on Emission Scenarios (SRES) - A2 (high) and B2 (low) emissions scenario. Ahmadisharaf *et al.* (2017) incorporated an integrated framework of a hydrologic model, a two-dimensional hydraulic model simulation, and a GIS-based technique for future flood hazard mapping of the Swannanoa River watershed in the U.S. If we focus on Asian countries, Shrestha & Lohpaisankrit (2017) assessed the flood hazard of the Yang River of Thailand for RCP 4.5 and RCP8.5. Gusain *et al.* (2020) recently studied the impacts of climate change on flood hazards of the Mahanadi River Basin of India under the RCP8.5 scenario. Though the world's research on future flood hazard and risk assessment is quite advanced, it has hardly been investigated in Bangladesh. Recently, Nishat (2017) developed the flood inundation map of the Brahmaputra River floodplain of Bangladesh for the warmest projection (RCP 8.5) considering the upstream basin-scale flood input from the Brahmaputra basin. However, it should be investigated for other flood-vulnerable rivers of the country as well.

Additionally, considering the flood threat of Bangladesh, an integrated flood risk assessment that connects the physical flood hazard with socio-economic aspects is necessary too. Previously, Das *et al.* (2018) quantified the future flood hazard of the Surma-Kushiara river system of Bangladesh, overlooking upstream basin runoff from the Meghna Basin. Brouwer *et al.* (2007) studied the socio-economic vulnerability and adaptation aspects of flooding in Bangladesh under climate change. However, all these studies either account for the hydrological characteristics of flood hazard or socio-economic context. Though few combined hazard and risk studies (Tingsanchali & Karim 2005; Ali *et al.* 2019) are conducted in the past, these studies are based on historic hydrologic data assuming stationarity of the climate, i.e., no shift in climate over time. Such risk assessment might underestimate the long-term impact of climate change (Milly *et al.* 2008). Hence, an integrated flood risk assessment for the flood-vulnerable rivers of Bangladesh under future climate emission scenarios is essential.

In this study, the climate change impact of two large upstream basins – Ganges and Brahmaputra (Figure 1(a)) with a combined area of approximately 1.6 million sq. km. has been incorporated in the local river Arial Khan through employing multiple numerical models to estimate the future flood scenarios at Arial Khan River and its floodplain. It is a river of the southwest zone of Bangladesh (shown in Figure 1(c)), the upper reach of which is subjected to riverine floods (Tingsanchali & Karim 2005). The river's water level was above the danger level (Figure 1(d)) during the big flood events - 1987, 1988, 1998, 2004, 2007, 2010, 2011, etc. of Bangladesh and caused tremendous sufferings to the people dwelling on its floodplain (FFWC 2018). The previous studies on the Arial Khan are centred on either morphological process or river erosion contexts (Winkley *et al.* 1994; Mamun 2008; Akter *et al.* 2013). No study focusing on integrated flood risk of the Arial Khan River is conducted yet. Considering these facts, the current study is designed to assess the integrated flood risk of the Arial Khan River using the IPCC AR5 risk framework considering both low and high emission scenarios. To achieve the scope, three specific objectives are fixed as – (i) to develop a multi-model hydrology-hydrodynamic modelling framework to assess the future flooding scenarios of the Arial Khan River (ii) to prepare flood hazard maps for the low (RCP 2.6) and high (RCP 8.5) emission scenarios, and (iii) to prepare integrated flood risk maps of Arial Khan River floodplain using IPCC AR5 risk framework.

While most of the studies in the past focus on either flood hazard or risk assessment, the novelty of the current research lies in assessing local-scale flood hazard incorporating upstream basin flows using RCP low and high emission scenarios, then connecting the physical flood hazard with socio-economic contexts in terms of vulnerability and exposure indices and finally assessing integrated flood risk using the most recent emission scenarios and climate risk framework proposed by the IPCC in AR5. Among all the RCP scenarios of Coupled Model Intercomparison Project 5 (CMIP5), the RCP2.6 and RCP8.5 are selected as being optimistic (low concentration) and pessimistic (high concentration) scenarios of the
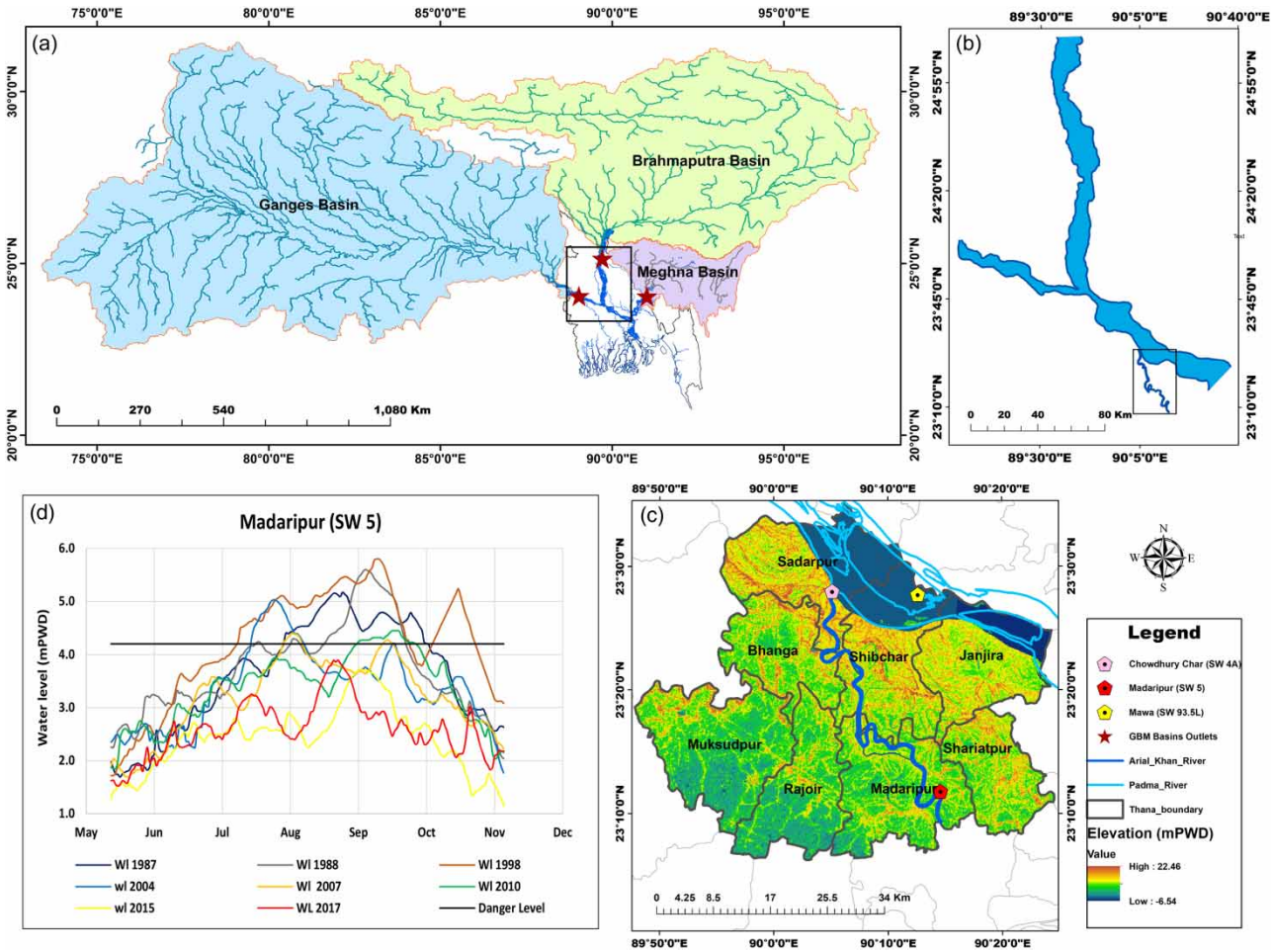
Figure 1 | Study area (a) Ganges-Brahmaputra-Meghna (GBM) Basins with their outlets in Bangladesh, (b) Brahmaputra-Ganges-Padma River system connected with the Arial Khan River, (c) Arial Khan River and floodplain and (d) Water level time series of Arial Khan River at d/s hydrological station (Madaripur SW 5) w.r.t. flood danger level.

future. The concept and associated definitions of hazard, exposure, vulnerability, and risk used in the present study are annexed in Supp. Table 1.

2. STUDY AREA

Bangladesh is the greatest deltaic plain at the confluence of the GBM rivers and their tributaries, covering an area of 1.7 million sq. km (Figure 1(a)). Being originated from the Himalayas of China, the Ganges and the Brahmaputra rivers flow through China and India, and then enter Bangladesh. Flowing some distance in Bangladesh, both the rivers join and form the Padma River (Figure 1(b)). Bifurcating from the Padma at Goalundo (Figure 1(c)), the Arial Khan River flows through Faridpur and Madaripur districts before falling into the Tentulia River (BWDB 2011).

The Arial Khan River maintains a meandering channel through its course and is navigable throughout the year. The total length of this river is 160 km, with an average width of 300 m and a bed slope of 0.00003 (BWDB 2011). The river has two parts: the Arial Khan Upper (AKU), and the other is called the Arial Khan Lower (AKL). The Arial Khan Upper and its adjacent floodplains are selected due to its existing problems with monsoon flood inundation (Tingsanchali & Karim 2005) [Figure 1(c)]. The reach length chosen considered in this study is 70 km. The floodplain of this portion of the river consists of eight Upazilas of four Districts – Madaripur, Shibchar and Rajoir Upazila of Madaripur District; Janjira, and Shariatpur Upazila of Shariatpur District; Bhanga, and Sadarpur Upazila of Faridpur District; and Maksudpur Upazila of Gopalgonj District. District and Upazila are served as the first- and second-level administrative units, respectively. For detailed analysis, Upazila is considered as the

land unit in this study. The total study area is nearly 1,825 km^2. The selected reach of the Arial Khan River is not protected by any flood embankment or coastal polder.

3. MATERIALS AND METHODS

3.1. Data

To develop the hydrodynamic models, the measured discharge, river cross-section, and water level data are collected from the BWDB. For the flood modelling, the 90 m SRTM DEM, measured w.r.t. Mean Sea Level (MSL) is used in the model. On the other hand, the river cross-section and water level are measured in Public Work Datum (PWD). Hence, the DEM has vertically translated from MSL to PWD by adding an elevation of 0.46 m. The Landsat-5 TM image is downloaded from the USGS website (Supp. Table 2). Exposure and vulnerability statistics are collected from the Population Census 2011 and Agriculture Census 2008 of the Bangladesh Bureau of Statistics (BBS 2020). These are the most recent demographic and socio-economic data currently available in Bangladesh. The different datasets used in this study are tabulated in Table 1.

3.2. Climate data

Climate studies are highly dependent on the climatic projections simulated by different Global Climate Models (GCMs) and Regional Climate Models (RCMs). The coarse resolution (100–200 km) of the GCMs of CMIP5 poses different limitations to simulate regional-scale climate impact. Though downscaled high-resolution RCMs with detailed spatial information address this gap, such dynamic downscaling requires another step of computation at a different regional modelling grid with boundary conditions set from lower resolution global scale GCM. Hence, it is computationally expensive and introduces additional uncertainties from physical parameterizations, boundary conditions, regional model setups, and bias corrections (Koutroulis et al. 2018). Hence, several studies suggested for GCMs with higher resolution that are able to simulate the observed energy spectrum of the climate system (Koutroulis et al. 2016; Zhang et al. 2016). To address these gaps, some improved and higher resolution Atmosphere Global Climate Models (AGCMs) is driven by a subset of CMIP5 GCMs and forced with Sea Surface Temperature (SST) and Sea Ice Concentration (SIC). 'EC-EARTH3-HR' (Hazeleger et al. 2011) is such an AGCM simulated under the HELIX project. It is bias-corrected data with a high spatial resolution of 0.5° (∼50 km). Mohammed et al. (2018) checked the quality of the climate data and used it to model future flow scenarios of Brahmaputra and Ganges basins in SWAT and found satisfactory results for both basins. Hence, this high-resolution and bias-corrected climate data is used in this study. However, since EC-Earth-HR is performed under the HELIX project for low (RCP2.6) and high (RCP8.5) emission scenarios only, it's not possible to explore this research for other RCP scenarios.

3.3. Model selection

A multi-model hydrology-hydrodynamic modelling framework is developed here to estimate future flooding scenarios in this study. There are many recognized hydrologic models such as HEC-HMS, SWAT, VIC, TOPMODEL, MIKE SHE, etc. The SWAT model is chosen here as it is a widely recognized open-source model for regional scales hydrological modelling due to its accuracy and flexibility (Mohammed et al. 2017). Many regional basin-scale hydrological studies have been

Table 1 | Summary of the environmental and socioeconomic datasets used in this study

Data Type	Location/Station Name/Station ID	Data Source
Daily precipitation and maximum and minimum temperature	Brahmaputra & Ganges basins	Princeton Global Forcing (version 2)
River bathymetry/cross-section	Brahmaputra, Ganges, Padma & Arial Khan River	BWDB
Discharge	Bahadurabad Transit (SW 46.9 L), Hardinge Bridge (SW 90), Mawa (SW 93.5 L) & Chowdhury Char (SW 4A)	BWDB
Water level	Bahadurabad Transit (SW 46.9 L), Hardinge Bridge (SW 90), Gualondu (SW 91.9R), Mawa (SW 93.5 L), Sureswar (SW 95), Chowdhury Char (SW 4A) & Madaripur (SW 5)	BWDB
Landsat-5 TM satellite image	Arial Khan River floodplain (Path/Row - 137/044)	USGS
Population statistics/Demographic socio-economic statistics	Faridpur, Gopalgonj, Madaripur & Shariatpur	BBS

conducted using SWAT since 2007 to date and appreciated for satisfactory results (Abbaspour *et al.* 2007; Solaymani & Gosain 2015; Rajib *et al.* 2020).

Among the hydrodynamic models, HEC-RAS, Delft3D, MIKE 11, LISFLOOD-FP, TU-Flow, etc., are some widely used numerical models. The hydrodynamic models are selected based on their application, spatial-temporal dimension, time-space-resource availability, etc. (Betancur-Pérez *et al.* 2016). 3D models are typically applied in small-scale coastal (Fossati & Piedra-Cueva 2013) or river modelling (Nicholas & McLelland 2004), fish pass (Gisen *et al.* 2017; Stamou *et al.* 2018), hydraulic structures (Nagata *et al.* 2005; Yang 2007), vortex analysis (Zhong *et al.* 1998), salinity (Larson *et al.* 2005), etc. Flood inundation mapping is a simple 2D overflow phenomenon. The vertical component is not crucial here. Application of a 3D model in such cases might cause complexities in the model setup and increase computational time, cost and space. Hence, large-scale flood inundation analysis is conducted with a 2D (Sutter 2019) or 1D/2D coupling (Rangari *et al.* 2019; Costabile *et al.* 2020). The open-source hydrodynamic model HEC-RAS is a widely used flood model due to its accuracy in analyzing river systems and recently added feature of 1D/2D river-floodplain coupling (Brunner 2016). The ability of HEC-RAS to perform combined 1D and 2D modelling within the same model allows 1D modelling in the main channel and 2D modelling in the floodplains (Brunner *et al.* 2015). As high-resolution river bathymetry data is practically non-existent in Bangladesh, the 1D/2D coupling provides a convenient trade-off between spatial accuracy and data requirements. Recently, many flood studies were conducted using HEC-RAS 1D/2D coupled model (Patel *et al.* 2017; Vozinaki *et al.* 2017; Das *et al.* 2018) and found satisfactory results.

3.4. Methodology

The primary objective of this study is to prepare flood hazard and risk maps for the Arial Khan River floodplain using a multi-model hydrology-hydrodynamic modelling framework under future climate change scenarios. A complete research methodology is illustrated in Figure 2 and described in the subsequent sections.

3.4.1. Regional hydrological modelling in SWAT

For a robust estimate of the future discharge scenarios, SWAT models of Ganges and Brahmaputra basins, developed by Mohammed *et al.* (2018) has been used here. SWAT model follows the basic water balance equation, as shown in Equation (1).

$$SW_t = SW_0 + \sum_{i=1}^{t} R_i - Q_i - ET_i - P_i - QR_i \tag{1}$$

where, SW_t is the final soil water content, t is time, SW_0 is the initial soil water content on day i, R_i is the amount of precipitation on day i, Q_i is the amount of the surface runoff on day i, ET_i is the amount of the evapotranspiration on day i, P_i is the amount of the percolation on day i, and QR_i is the amount of return flow on the day i.
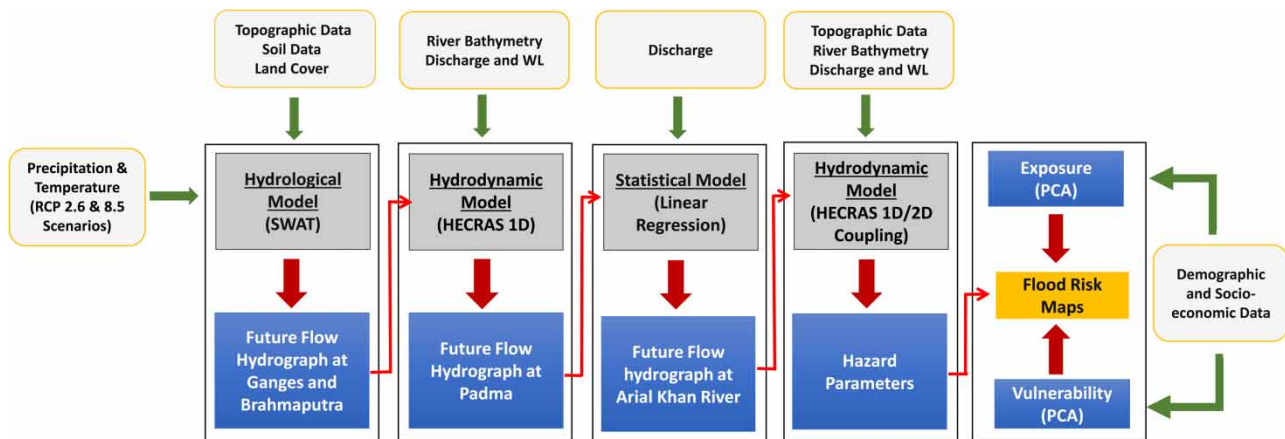

Figure 2 | Flow diagram showing the research methodology.

The SWAT model has been developed using 90 m DEM from HydroSHEDS, GlobCover land-use map from ESA, digital soil-map from FAO, and meteorological data from Princeton Global Forcing. The performance of the model is graphically shown in Supp. Figure 1 and statistically quantified in Supp. Table 3. More details on the SWAT model development, sensitivity analysis, calibration, and validation are found in Mohammed *et al.* (2018).

3.4.2. Hydrodynamic modelling in HEC-RAS

The hydrodynamic modelling framework used here is HEC-RAS 5.0.1, developed by the US Army Corps. For 1D unsteady analysis, HEC-RAS solves 1-D Saint Venant Equation derived from Navier-Stokes Equations for shallow water flow conditions using an Implicit Finite Difference method. For 2D analysis, HEC-RAS uses the Implicit Finite Volume algorithm and solves either full 2D Saint Venant equations or 2D Diffusion Wave equations as defined in Equations (2)–(4) depending on the requirement and preference (Brunner 2016; Quiroga *et al.* 2016).

$$\frac{\delta \zeta}{\delta t} + \frac{\delta \rho}{\delta x} + \frac{\delta q}{\delta y} = 0 \tag{2}$$

$$\frac{\delta \rho}{\delta t} + \frac{\delta}{\delta x}\left(\frac{p^2}{h}\right) + \frac{\delta}{\delta y}\left(\frac{pq}{h}\right) = -\frac{n^2 pg\sqrt{p^2 + q^2}}{h^2} - gh\frac{\delta \xi}{\delta x} + pf + \frac{\delta}{\rho \delta x}(h\tau_{xx}) + \frac{\delta}{\rho \delta y}(h\tau_{xy}) \tag{3}$$

$$\frac{\delta q}{\delta t} + \frac{\delta}{\delta y}\left(\frac{q^2}{h}\right) + \frac{\delta}{\delta x}\left(\frac{pq}{h}\right) = -\frac{n^2 qg\sqrt{p^2 + q^2}}{h^2} - gh\frac{\delta \xi}{\delta y} + qf + \frac{\delta}{\rho \delta y}(h\tau_{yy}) + \frac{\delta}{\rho \delta x}(h\tau_{xy}) \tag{4}$$

where h is the water depth (m), p and q are the specific flow in the x and y-direction ($m^2 s^{-1}$), ξ is the surface elevation (m), g is the acceleration due to gravity (ms^{-2}), n is the Manning resistance, ρ is the water density ($kg\ m^{-3}$), τ_{xx}, τ_{yy} and τ_{xy} are the components of the effective shear stress and f is the Coriolis (s^{-1}).

3.4.2.1. HEC-RAS 1D Model. An HEC-RAS 1D model is developed to simulate the upstream boundary flow to the HEC-RAS 1D/2D flood model (Supp. Figure 2). This 1D model has been set up for the Ganges, Brahmaputra, and Padma River system using Bahadurabad Transit and Hardinge Bridge as upstream boundaries and Sureswar as a downstream boundary. The u/s discharge boundaries and d/s water level boundary used for model calibration and validation are shown in Supp. Figure 3(a) and 3(b).

3.4.2.2. Statistical Modelling. The Padma is the parent river (only contributor as well) of the Arial Khan. The hydrology of the Arial Khan River follows almost the same pattern as the Padma River (FFWC 2018). A statistical regression model is developed between the discharge at Mawa of the Padma River to that of Chowdhury Char of the Arial Khan River. Mawa station of the Padma River is the closest station (10 km away) to the Chowdhury Char of the Arial Khan River. The other closest station is nearly 40 km away at Bauria Transit which is also the confluence of two mighty rivers, Brahmaputra and Ganges, making its flow disturbed. Hence, it is not appropriate for this purpose.

3.4.2.3. HEC-RAS 1D/2D coupled Flood Model. For the 1D river modelling, the bathymetry is set up using HEC-GeoRAS and HEC-RAS (Supp. Figure 4 (a), (b)). Later, the daily discharge and water level of Chowdhury Char and Madaripur are used as model boundaries (Supp. Figure 3c and 3d). For the 2D floodplain, a square gridded – mesh is prepared in HEC-RAS Geometry Editor. Though a smaller mesh size increases the flood accuracy, it increases the computational time and space in return. After several trials and errors, a square mesh of 150 m is used for this study. Among six peripheral boundaries (Supp. Figure 4 (c)), two boundaries are added to the left edge to incorporate the flood impact of the neighbouring Padma River. The rest of the boundaries (with a normal depth of 0.1 m) are added to the lower periphery to remove the stagnant floodwater during the recession period. Lateral structures are set up along the river banks to create connections between the 1D river and the 2D floodplain.

After the model simulation, three flood parameters – flood depth (m), duration (days), and flood extent (m^2) are drawn out from the model. Flood depth (m) and area (m^2) are extracted for their maximum value. The duration is computed when water depth exceeds a specified threshold flood depth of 0.6 m. The result of the flood modelling is then used as the input in flood hazard assessment described in section 3.6.

3.5. Model performance evaluation

The performance of the hydrodynamic and statistical models is evaluated using statistical indicators – Nash Sutcliffe Efficiency (NSE), Coefficient of Determination (R^2), and Normalized Root Mean Square Error (NRMSE). These are the most widely accepted indices used for evaluating the performance of hydrodynamic models. Threshold values of the statistical indicators are taken from Moriasi *et al.* (2007).

NSE is a normalized statistic that determines the relative magnitude of the residual variance compared to the observed data variance. It ranges from 1 to -∞ with 1 as the optimum value. It is defined as:

$$NSE = 1 - \left[\frac{\sum_{i=1}^{n} (y_i^{obs} - y_i^{sim})^2}{\sum_{i=1}^{n} (y_i^{obs} - y_{mean}^{obs})^2} \right] \tag{5}$$

R^2 determines the proportion of the variance in the dependent variable that is predicted from the independent variables. It ranges from 0 to 1, with 1 as the optimum value. It is defined as:

$$R^2 = \left[\frac{\sum_{i=1}^{n} (y_i^{obs} - y_{mean}^{obs})(y_i^{sim} - y_{mean}^{sim})}{\sqrt{\sum_{i=1}^{n} (y_i^{obs} - y_{mean}^{obs})^2} \sqrt{\sum_{i=1}^{n} (y_i^{sim} - y_{mean}^{sim})^2}} \right]^2 \tag{6}$$

Normalized Root Mean Square Error (NRMSE) is used in this study to quantify the error between the observed values and model simulated values using the following equation [Equation (7)]:

$$NRMSE = \left[\frac{1}{n} \sum_{i=1}^{n} \left(\frac{y_i^{obs} - y_i^{sim}}{y_i^{obs}} \right)^2 \right]^{1/2} \tag{7}$$

where, y_i^{obs} is the ith observed value for the constituent, y_i^{sim} is the ith simulated value for the constituent, y_{mean}^{obs} is the mean of the observed data, y_{mean}^{sim} is the mean of the simulated data, and n is the total number of observations.

3.6. Hazard assessment

One or more parameters, such as flood depth, duration, inundation area, wave velocity, and rate of rising of water level (i.e., tide), are usually used to estimate flood hazards (Tingsanchali & Karim 2005). The hazard parameters are selected based on the characteristics of the area (UN 1991). Arial Khan floodplain is a part of the southwest river system of Bangladesh. This region is a large floodplain with flat topography (average % rise of SRTM DEM is 1.128; Supp. Figure 5), implying that the impact of velocity is very low here. Analyzing the historical observed water level data, the average tidal range is found less than 0.1 m at the model downstream boundary (Madaripur station) during the flood season. Hence, the flood flow velocity, wave velocity, and tide level are not hazard dominating factors over the study area. Considering the study area characteristics, three hazard parameters, (a) flood depth, (b) duration, and (c) area, are preliminarily selected for the hazard assessment. A sensitivity analysis is also conducted, showing how the parameters are influencing the resulting hazard maps.

3.6.1. Hazard index (HI)

The HI is the intensity of flood hazards. Each hazard category of different parameters is given a linear index from 1 to 5. A larger index means higher hazard, while a smaller hazard index means lower hazard. Among the available flood depth classifications, Agro-ecological Zone Land classification by FAO and Flood classification by National Water Management Plan (NWMP) are widely used in Bangladesh. Agro-ecological zone land classes are used for agricultural purposes. NWMP classification is used by the Flood Forecasting and Warning Center (FFWC) of BWDB, which is the officially mandated government organization of Bangladesh for all kinds of food-related studies. Considering the purpose of this study, the flood depths are classified following the NWMP guidelines. The hazard classification for the duration of flooding used

Table 2 | Hazard index for the selected hazard indicators

Depth of Flooding (m)	Category	HI	Duration of Flooding (day)	Category	HI	Area Inundated (%)	Category	HI
D ≤ 0.3	Very Low	1	T ≤ 3	Short	1	0 < A ≤ 20	Very Low	1
0.3 < D ≤ 0.9	Low	2	3 < T ≤ 7	Medium	2	20 < A ≤ 40	Low	2
0.9 < D ≤ 1.8	Medium	3	7 < T ≤ 25	Long	3	40 < A ≤ 60	Medium	3
1.8 < D ≤ 3.6	High	4	25 < T	Very Long	4	60 < A ≤ 80	High	4
D > 3.6	Very High	5				80 < A ≤ 100	Very High	5

here has been followed by Tu & Tingsanchali (2010). The % of area inundated is computed as the percentage of the total area of that Upazila. The hazard index classification followed in this study is given in Table 2.

3.6.2. Mean hazard index (MHI)

The MHI of each land unit (here, Upazila) is calculated, independently, for depth and duration, considering the percentage of land area under each category as given by Equation (8):

$$\text{MHI} = \frac{\left(\sum_{i=1}^{n} \text{HI}_i \, LA\right)}{\sum_{i=1}^{n} LA} \tag{8}$$

where, HI_i is the hazard index of land area LA_i of hazard category i, and n is the total number of land areas in the land unit.

3.6.3. Hazard factor (HF)

The HF represents the combined flood effect due to flooding depth, duration, and area in a land unit, as shown in Equation (9).

$$\text{HF} = a*\text{MHI}_{\text{depth}} + b*\text{MHI}_{\text{duration}} + c*\text{MHI}_{\text{inundation area}} \tag{9}$$

where $\text{MHI}_{\text{depth}}$ and $\text{MHI}_{\text{duration}}$ are the weighted average hazard index for flooding depth and duration, respectively, and $\text{MHI}_{\text{inundation area}}$ is the arithmetic average hazard index for flooding area. a, b, and c are the weightage factors of the hazard parameters.

3.7. Exposure and vulnerability assessment

3.7.1. Indicator selection

The Exposure and Vulnerability indices are selected following the concept of IPCC AR5. The selection is based on hazard type, data availability, expert opinion, local communities, livelihoods, etc. Later, this list has been improved by looking into recent literature (Kabir et al. 2017; Jahan 2018; Uddin et al. 2019). In total, 3 exposure and 12 vulnerability indicators are selected. The exposure indicators are – 1. Population Density, 2. No. of Household, and 3. Cropped Land. Among the vulnerability indicators, there are 4 Sensitivity indicators (1. Disable Population, 2. Dependent Population Ratio, 3. Female to Male Ratio, and 4. Poverty Rate), and 8 Adaptive Capacity indicators (1. Pucca and Semi-Pucca House[1], 2. Communication Infrastructure, 3. Crop Productivity, 4. Literacy Rate, 5. Health Centre, 6. Flood Shelter, 7. Growth Centre, and 8. Flood Forecasting & Warning System). The Sensitivity indicators give positive (+)[2] dependency on estimating vulnerability, while Adaptive capacity provides the negative (-)[2] dependency. This approach of quantifying vulnerability in terms of positive and negative dependence is introduced by Cutter et al. (2003) and later used by Allen et al. (2016) and Jahan (2018) for vulnerability assessment.

---

[1] A pucca house is one that has walls and roof made of pucca material such as bricks, stones, cement concrete, timber, etc and Semi -Pucca house: A house that has fixed walls made up of pucca material but roof is made up of the material other than those used for pucca house

[2] A positive (+) dependency means that an increase in the variable indicates an increase in vulnerability, whereas a negative (–) dependency means that an increase in the measured variable indicates a decrease in vulnerability.

3.7.2. Normalization of the indicators

Normalization ensures comparability among the indicators regardless of their units of measurement (Kabir *et al.* 2017). A normalized index is established with dimensionless values ranging from 1 (indicating low value) to 100 (indicating high value) for each indicator of exposure and vulnerability. For each indicator (I), Upazila values (I_t) are normalized (I_{nor}) to values in a common range of 1 to 100 using Equations (10) and (11) as used by (Jahan 2018).

$$I_{nor} = 1 + \frac{(I_t - I_{min})(100 - 1)}{(I_{max} - I_{min})} \tag{10}$$

Higher value of I_{nor} indicates higher vulnerability (positive dependency).

$$I_{nor} = 1 + \frac{(I_{max} - I_t)(100 - 1)}{(I_{max} - I_{min})} \tag{11}$$

Higher value of I_{nor} indicates reduced vulnerability (negative dependency).

3.7.3. Weightage of the indicators

The weightage of indicators is provided to ensure that the most significant indicators are given more importance than the others (Kabir *et al.* 2017). Equal Weighting (Sarkar *et al.* 2019), Expert Weighting (Ahsan & Warner 2014), Participatory Rural Appraisal (PRA) (Younus 2017), Analytical Hierarchy Process (AHP) (Lappas & Kallioras 2019), Principal Component Analysis (PCA) (Uddin *et al.* 2019) are widely used weightage methods for socio-economic vulnerability assessment in Bangladesh. Expert weighting, PRA, AHP provide better results for the small-scale weightage selection process (Jahan 2018). However, none of these approaches satisfactorily quantifies large-scale weight assessment as they highly depend on human judgment, sample size, and techniques and are computationally expensive. In these particular cases, statistical methods are considered to be more scientifically defensible, unbiased towards expert opinion and local perception, and less resource-intensive. PCA is such a statistical method that extracts a smaller and more coherent set of uncorrelated (orthogonal) factors from a large number of variables, where the first component accounts for the largest possible amount of variation in the original variables, and each succeeding component accounts for as much of the remaining variability as possible (Gbetibouo *et al.* 2010). Hence, PCA is used to provide Upazila-wise weightage to the indicators. After assigning weights using PCA, the Exposure and Vulnerability of each of the Upazilas are calculated by using Equations (12) and (13).

$$\text{Exposure} = W_1 * I_{EX1} + W_2 * I_{EX2} + W_3 * I_{EX3} + \ldots\ldots\ldots\ldots W_n * I_{EXn} \tag{12}$$

$$\text{Vulnerability} = W_1 * I_{v1} + W_2 * I_{v2} + W_3 * I_{v3} + \ldots\ldots\ldots\ldots W_n * I_{vn} \tag{13}$$

where W is the weight of the indicator, I_{EX} is the normalized indicator of exposure, and I is the normalized indicator of vulnerability. Suffix 1,2…..n are used to represent each item, and n is the total number of items.

3.8. Integrated risk assessment

Finally, flood risk (R) is calculated as the consequence of the physical hazard (H), intersecting with vulnerability (V) and exposure (E) following the IPCC AR5 risk framework as shown in Equation (14) (IPCC 2014; Allen *et al.* 2016).

$$R = H * E * V \tag{14}$$

3.9. Post-Processing in ArcGIS

Hazard, exposure, vulnerability, and risk indices are normalized and classified into five categories maintaining an equal interval for each case, 0–20, 20.01–40, 40.01–60, 60.01–80, and 80.01–100 for Very Low, Low, Medium, High and Very High respectively. Finally, the Upazila-wise hazard, exposure, vulnerability, and risk maps are prepared in ArcGIS.

4. RESULTS AND DISCUSSION

4.1. Calibration and validation of developed models

4.1.1. Calibration & validation of HEC-RAS 1D model

The 1D HEC-RAS model for the Ganges-Brahmaputra-Padma (GBP) river has been calibrated and validated using the observed flow at the Mawa station for four months from July to October for the year 2016 and 2017, respectively. Flow at Mawa station is chosen since it is later used for developing statistical regression models between Arial Khan Offtake and Padma. Here, the model's sensitivity has been tested by changing Manning's roughness coefficient n value for the model and comparing the change in maximum discharge at Mawa station. The relation between Manning's n value and corresponding maximum discharge at Mawa shows discharge decreases for a higher Manning's n value (Figure 3(c)). An increase in Manning's n value of 0.005 results on average 1,074.31 m^3/s decrease in maximum discharge. After checking that the model is sensitive to Manning's n, four sets of Manning's n as (0.015–0.02), (0.02–0.025), (0.025–0.03), and (0.03–0.035) are adopted to calibrate the model for the main channel and both left and right banks. The comparison of observed and simulated flow at Mawa (SW 93.5 L) station for various Manning's n and corresponding statistical performance is presented in Table 3a. The simulated discharge hydrographs for $n = 0.015$–0.02 and $n = 0.02$–0.025 do not match the observed discharge in the beginning and end of the year, and there are some outliers in the simulated values. The trend and shape of the simulated and observed hydrograph are almost similar for n as 0.025–0.03 and n as 0.03–0.035. Finally, n as 0.025 for the main channel and n as 0.03 for the banks have been fixed as it gives the most acceptable values of R^2 and NSE. The values of R^2 and NSE have been found to be 0.9168 and 0.9138, respectively, indicating that the simulated value is very close to the observed value and within the acceptable range. Using the calibrated Manning's n, validation has been performed for the year 2017. Figure 3(f) shows the simulated flow hydrograph is in close agreement with the observed flow hydrograph. In this case, the coefficient of determination R^2 and NSE have been found 0.8212 and 0.7424, respectively, which indicates that the validated value is closer to the observed value (Table 3a).

4.1.2. Performance of regression model

A statistical regression model is developed between the discharge at Mawa of the Padma River to that of Chowdhury Char of the Arial Khan River. Five different regression models: Linear, Exponential, Logarithm, Polynomial, and Power, are tried using the observed discharge data for the monsoon period of the year from 1965 to 2017 (Figure 3(a) & Table 4). A two-tailed Student T-test is conducted at a 5% significance level to check the quality of the data obtained from differential equations. For T-test,

- The null hypothesis (H0) assumes that the difference between the true (observed) mean (μ) and the comparison (model) mean (m0) is equal to zero (H0: $\mu = $ m0). i.e., no significant difference in the observed mean and model mean.
- The alternative hypothesis (H1) assumes that the difference between the true mean (μ) and the comparison mean (m0) is not equal to zero (H1: $\mu \neq $ m0), i.e., a significant difference exists between the observed mean and model mean.

If the *p*-value is less than significance level alpha $= 0.05$, we reject the null hypothesis. On the other hand, if the *p*-value is greater than alpha $= 0.05$, we accept the null hypothesis. The *p*-values of Exponential (7.1044E-190), Polynomial (0.01008314), and Power (1.08119E-06) are less than alpha. Hence, we reject the null hypothesis, i.e., the population means are different. On the other hand, the *p*-values of Linear (0.945843311) and Logarithmic (0.986220415) are greater than alpha 0.05. Hence, we can accept the null hypothesis, i.e., that the population means are the same. The linear Equation (Equation (15)) is selected for further investigation based on the NSE and R^2 values among the Linear and Logarithmic equations.

$$Q_{\text{Arial Khan}} = 0.0358 * Q_{\text{Padma}} - 281.03 \tag{15}$$

where $Q_{\text{Arial Khan}}$ and Q_{Padma} are the discharge of Chowdhury Char and Mawa.

The 95% confidence and prediction interval are estimated for the selected linear regression equation (Figure 3(b)) to quantify the uncertainty. Here, the confidence interval shows the uncertainty involved in predicting mean response at 95% confidence interval that means it is 95% confident that the mean discharge of Arial Khan will fall in this range. On the
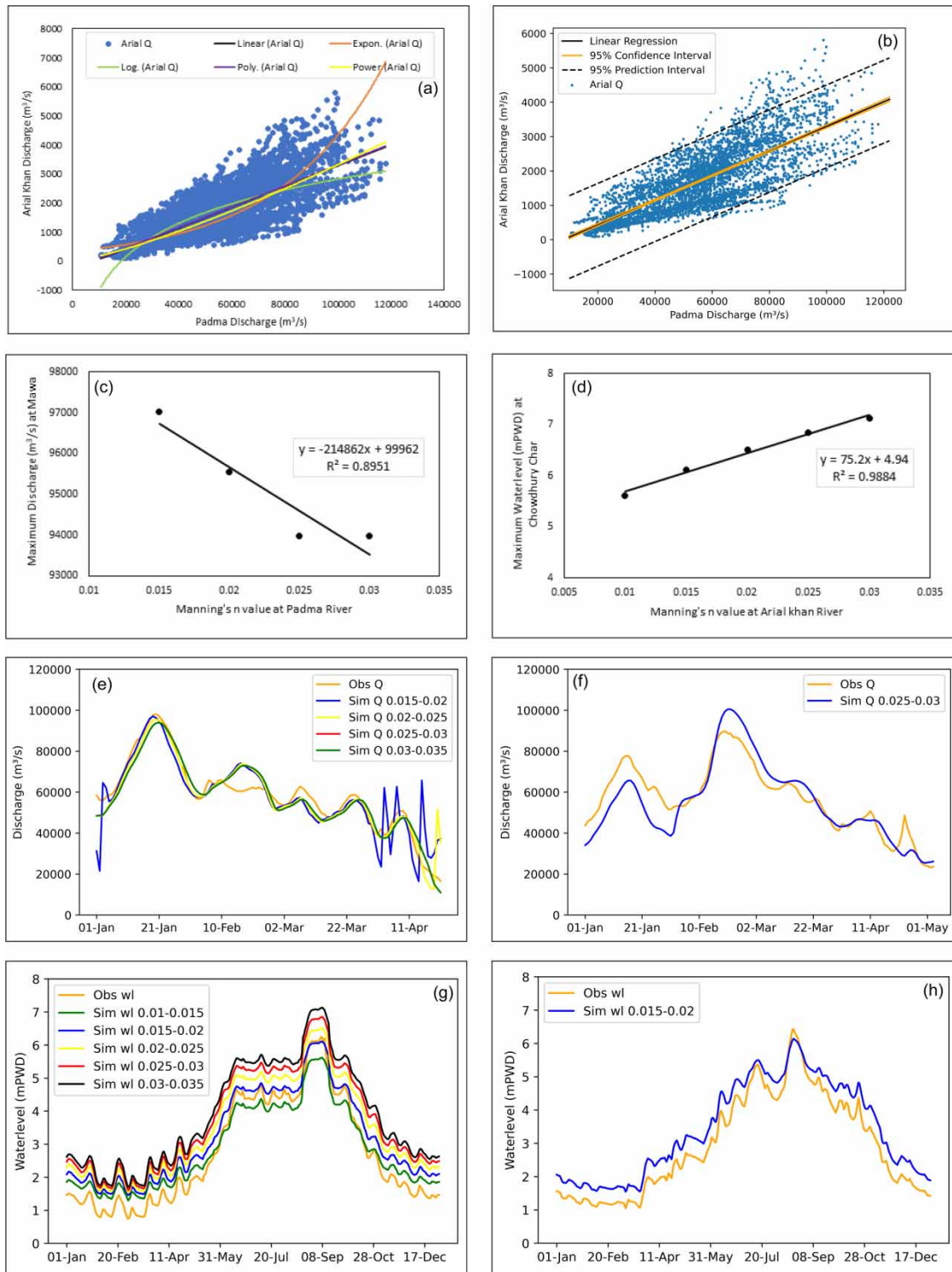
Figure 3 | Performance evaluation of the developed models (a) different statistical regression models between Arial Khan River and Padma River, (b) confidence and prediction interval for the selected linear regression model (c) change in discharge due to change in Manning's *n* value of Ganges-Brahmaputra-Padma River HEC-RAS model at the Padma River (d) change in water level due to change in Manning's n value of Arial Khan HEC-RAS model (e) calibration and (f) validation of GBP model, (g) calibration and (h) validation of the Arial Khan model.

Table 3 | Performance evaluation of the hydrodynamic model HEC-RAS

Model	Period	Calibration Location	Trials	Manning's Roughness Coefficient (n) Main Channel	Banks	Performance Evaluation NSE	Performance	R^2	Performance
(a) Ganges-Brahmaputra-Padma River System	Calibration (2016)	Padma River (Mawa-SW 93.5 L)	1	0.015	0.020	0.7327		0.7501	
			2	0.020	0.025	0.8861		0.8894	
			3	0.025	0.030	0.9138	very good	0.9168	very good
			4	0.030	0.035	0.9136		0.9166	
	Validation (2017)	Padma River (Mawa-SW 93.5 L)	–	0.025	0.030	0.74	good	0.9974	very good
(b) Arial Khan River	Calibration (2015)	Arial Khan River (Chowdhury Char – SW 4A)	1	0.010	0.015	0.943		0.9974	
			2	0.015	0.020	0.892	very good	0.9952	very good
			3	0.020	0.025	0.775		0.9929	
			4	0.025	0.030	0.630		0.9908	
			5	0.030	0.035	0.471		0.9974	
	Validation (2017)	Arial Khan River (Chowdhury Char – SW 4A)	–	0.015	0.020	0.88	very good	0.99	very good

Table 4 | Performance of different statistical models developed between Padma and Arial Khan

No.	Regression model	Equation	Two-tailed T test at 5% significance level P value	Comment	NSE	R^2
1	Linear	$y = 0.0358x - 281.03$	0.94584	Accept Null Hypothesis, Mean is same, Acceptable	0.59921	0.59920
2	Exponential	$y = 343.78e^{3E\text{-}05x}$	7.10E-190	Reject Null Hypothesis, Mean is not Same, Not Acceptable	−0.56896	0.52940
3	Log	$y = 1663.4\ln(x) - 6326$	0.98622	Accept Null Hypothesis, Mean is same, Acceptable	0.55589	0.55590
4	Polynomial	$y = 7E\text{-}09x^2 + 0.035x - 261.32$	1.01E-02	Reject Null Hypothesis, Mean is not same, Not Acceptable	0.59830	0.59920
5	Power	$y = 0.0014x^{1.2779}$	1.08E-06	Reject Null Hypothesis, Mean is not same, Not Acceptable	0.59421	0.59740

other hand, the prediction interval shows the range of uncertainty in predicting a single response at a 95% confidence interval that means it is 95% confident that any discharge of Arial Khan will fall in this range.

4.1.3. Calibration & validation of HEC-RAS flood model

The 1D model of the Arial Khan flood model has been calibrated using the observed daily water level data at Chowdhury Char station for twelve months from January to December of 2015. The model's sensitivity has been tested by changing the Manning's n value for the Arial Khan River and comparing the change in maximum water level at Chowdhury Char. The relation between Manning's n and corresponding maximum water level at Chowdhury Char shows water level increases for a higher Manning's n value (Figure 3(d)). An increase in Manning's n value of 0.005 results on average 0.38 mPWD increase in maximum water level. After checking the sensitivity, five sets of Manning's n as (0.010–0.15), (0.015–0.02), (0.02–0.025), (0.025–0.03), and (0.03–0.035) are adopted to calibrate the model. Comparison between the observed and simulated stage hydrographs for different sets of Manning's 'n' shows that the trend and shape of the observed and simulated hydrographs are almost similar (Figure 3(g)). The simulated hydrograph of n as 0.015 for the main channel and n as 0.02

for the left and right banks matches more accurately with the observed hydrograph. The simulated water level and observed water level almost matches in monsoon from June to September. The model overestimates during the dry season from October to May. However, as the main focus of this study is monsoon flood hazard assessment, this discrepancy does not affect the final results.

Among different sets of roughness values, the R^2 and NSE values of n as 0.01–0.015 have been found 0.9974 and 0.943, and the R^2 and NSE values of n as 0.015–0.02 have been found 0.9974 and 0.892. The visual observation shows that 0.015–0.02 more accurately captures the monsoon season flow than 0.01–0.015. Hence, n as 0.015–0.02 has been fixed as Manning's 'n' for all the cross-sections of the Arial Khan River. Using the calibrated Manning's n, model validation has been performed for the year 2017. The validation has also shown satisfactory results. Figure 3(h) shows that the simulated stage hydrograph is in close agreement with the observed hydrograph. There were slight differences in simulated water level and observed water level in the dry season like calibration. In the validation, the coefficient of determination R^2 and NSE have been found 0.989 and 0.882, respectively, which indicates a good correlation between the observed and simulated data and indicates the model's accuracy for further analysis.

4.1.3.1. Comparison of 2D Flood Inundation. The 2D flood inundation is validated comparing with the available satellite images. The simulated flood inundation map on 25 August 2004 is validated by comparing the flood inundation map derived from the Landsat-5 TM satellite image taken on the same day, as shown in Figure 4. The model flood map shows a significant flood around the Arial Khan River, which agrees with the Landsat map of that day. Additionally, a quantitative comparison of the flood inundation area has been made between Landsat and Simulated flood map based on NDWI (Normalized Difference Water Index). The flood area found from the satellite image, and the simulated model is 550.76 km^2 (26% of the study area) and 510.11 km^2 (24% of the study area). Upazila-wise, the floods in Janjira, Shibchar, Madaripur, and Bhanga highly coincide with the satellite image. However, the flood in Sadarpur is slightly overestimated, and the floods in Shariatpur and Madaripur are somewhat underestimated. The flooding along the main channel was accurately simulated as the upstream discharge was accurately estimated through the above-mentioned hydrological and hydrodynamic models. However, since the local rainfall is not dynamically incorporated in the 2D modelling, the model couldn't appropriately capture the flood in the peripheral depressions filled by the local rain. Hence, flood in the periphery of the study area (especially the southwest and southeast zone) was slightly underestimated.

4.2. Climate change projections

The calibrated and validated Ganges-Brahmaputra SWAT model is simulated with the EC-EARTH3-HR data from 1976 to 2100 for RCP2.6 and RCP8.5 scenarios and daily flow hydrographs are extracted. The hydrographs show that the future flow for RCP2.6 and 8.5 is similar from 1976 to 2040 (Supp. Figure 6). After that, the future flow for the RCP8.5 scenario is significantly higher than that of RCP2.6 for both of the basins.

From SWAT simulations, three thirty-year long time slices are considered for each of the RCP scenarios – the early (2020s z; 2006–2035), the mid (2050s: 2036–2065), and the end (2080s: 2066–2095) of the 21st century. The climate data typically
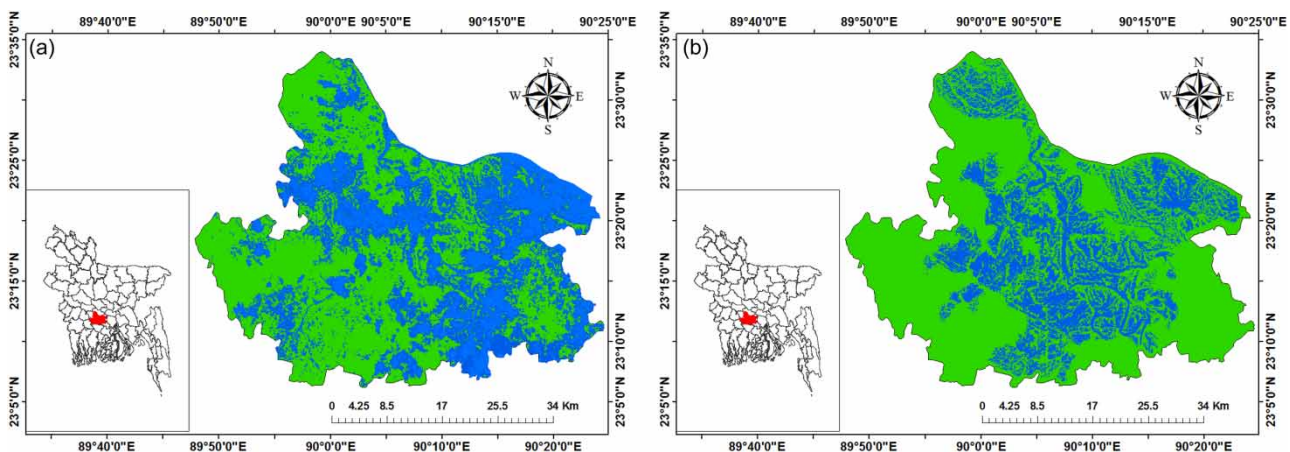

Figure 4 | Qualitative comparison of inundation map prepared using (a) Landsat-5 satellite images and (b) simulated model.

contains a lot of outliers. So, extreme flood scenarios are assessed by the 90th percentile rather than the mean or maximum of the dataset (Bonsal *et al.* 2001). This concept has been used in many climate studies to generate future climate scenarios (Beniston *et al.* 2007; Braun *et al.* 2014). Hence, the 90th percentile daily flow hydrographs for each of the mentioned time slices under RCP 2.6 and 8.5 scenarios have been extracted, as shown in Figure 5. Later on, these hydrographs have been used as the future u/s discharge boundaries of the HEC-RAS 1D model.

4.3. Projected changes in floods

The projected flood parameters are extracted, and flood maps for different time periods under RCP2.6 and RCP8.5 are prepared in ArcGIS (Figure 6). An increasing trend in the flood area, depth, and duration are observed from the 2020s to the 2080s for RCP2.6 and RCP8.5 scenarios. The difference between RCP2.6 and RCP8.5 is not significant from the 2020 to 2050 s. However, the difference becomes very prominent after the 2050s. At the end of the 21st century, the total inundated area is nearly 523 km^2 (29% of the total area) under RCP2.6, while it is almost 800 km^2 (44% of the total area) under RCP8.5.

In total, 6 Upazilas (Sadarpur, Madaripur, Rajoir, Shibchar, Shariatpur, and Zanjira) out of 8 Upazilas is flooded in the 2020s of RCP2.6 and RCP8.5 (Table 5). The flood in Shariatpur is very insignificant. No flood is found in Bhanga and Maksudpur Upazilas. However, the flooding scenario changes with time, especially it significantly exacerbates after the 2050s. At
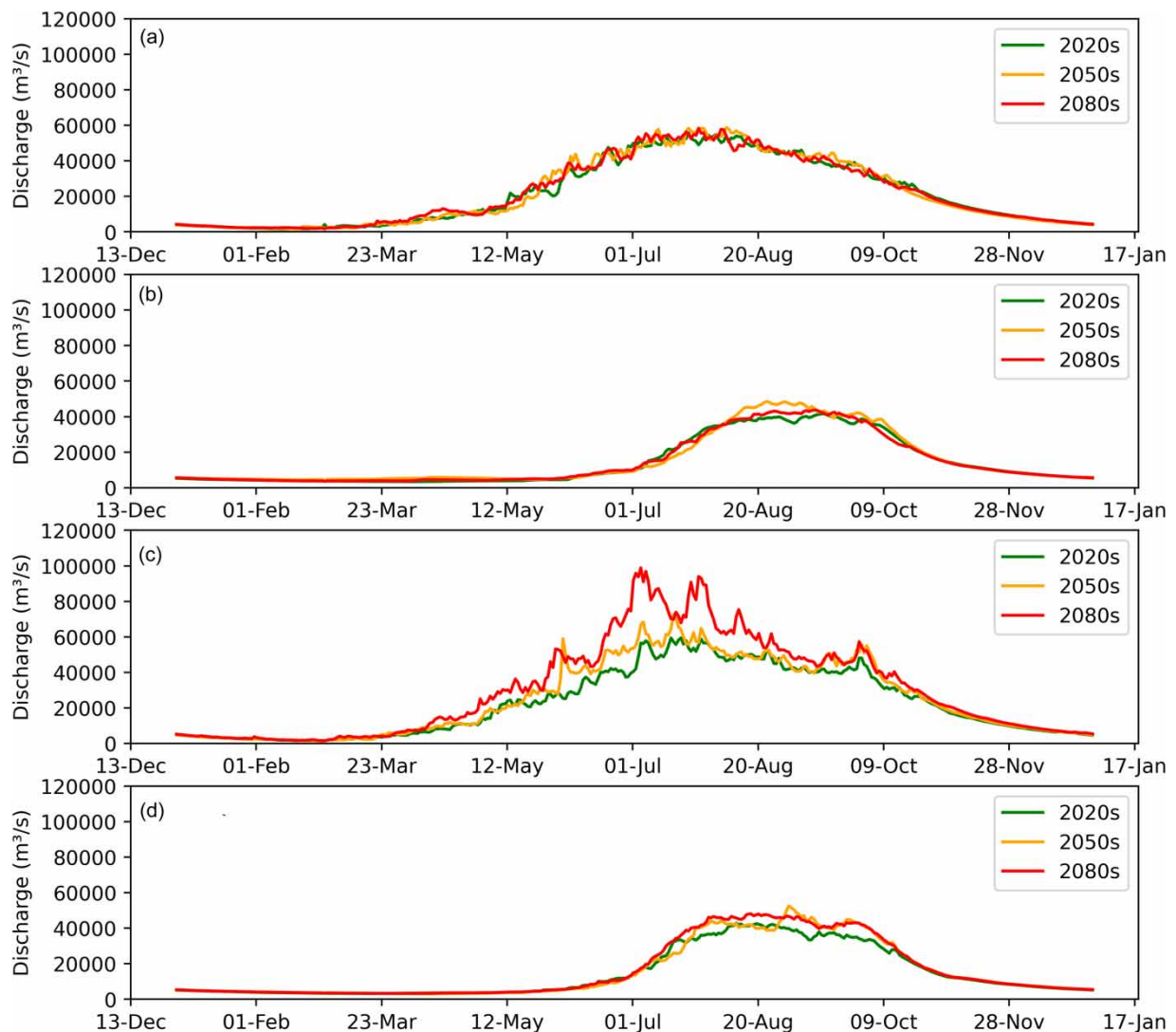

Figure 5 | 90th percentile daily flow hydrograph for the 2020s, 2050s, 2080s (a) the Brahmaputra and (b) Ganges for RCP2.6 (c) the Brahmaputra and (d) Ganges for RCP8.5.
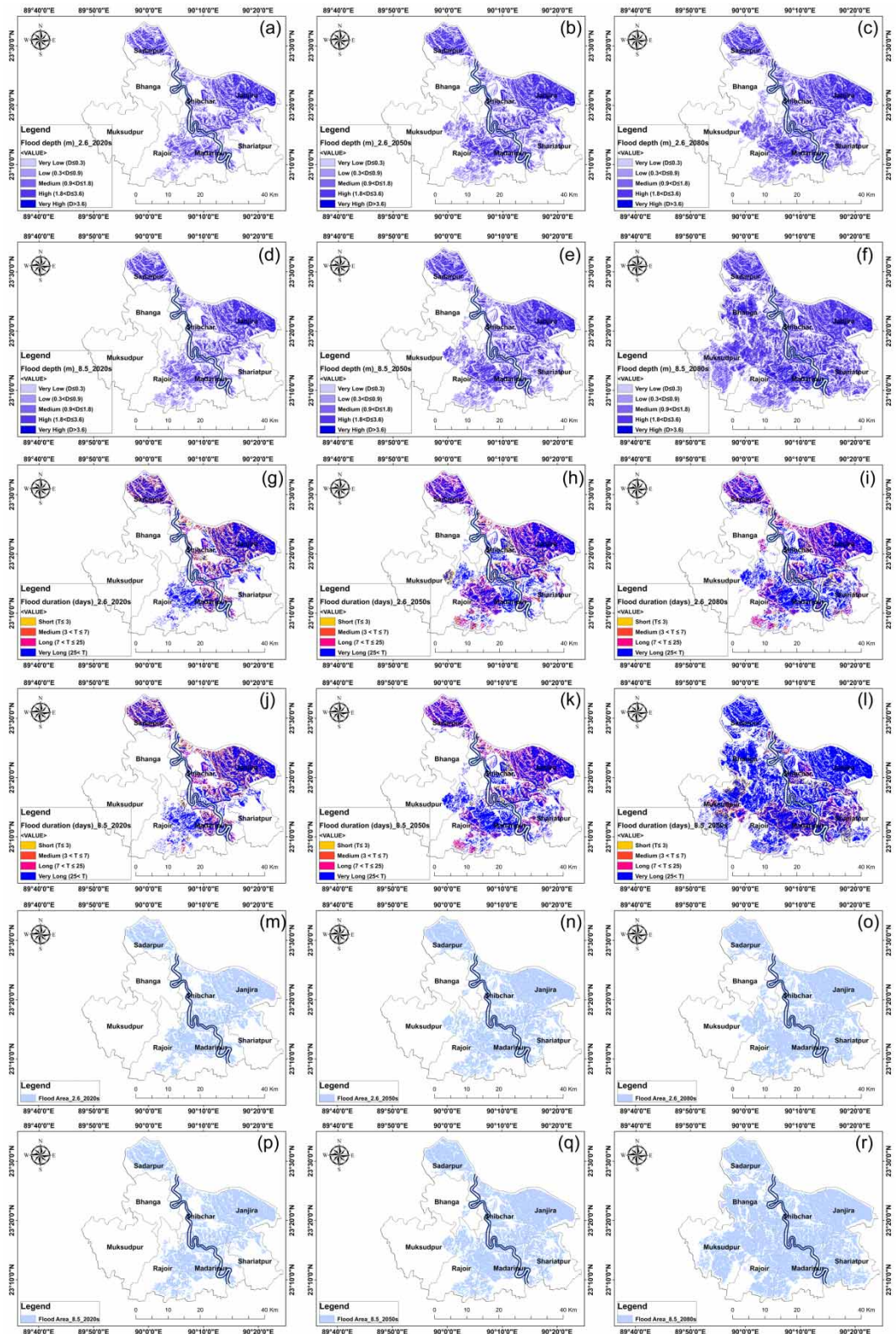
Figure 6 | Flood depth in (a) 2020s (b) 2050s (c) 2080s under RCP2.6 and in (d) 2020s (e) 2050s (f) 2080s under RCP8.5; Flood duration in (g) 2020s (h) 2050s (i) 2080s under RCP2.6 and in (j) 2020s (k) 2050s (l) 2080s under RCP8.5; Flood extent in (m) 2020s (n) 2050s (o) 2080s under RCP2.6 and in (p) 2020s (q) 2050s (r) 2080s under RCP8.5.

the end of the 21st century, the flood-affected areas are 5, 76, 17, 113, 55, 73, 45, and 138 km^2 under RCP2.6 and 100, 81, 109, 131, 84, 94, 60 and 139 km^2 under RCP8.5. Therefore, it can be inferred that the flood-affected area will increase significantly in both RCP8.5 due to climate change.

4.4. Sensitivity of flood hazard parameters

The sensitivity analysis of the hazard parameters is important to assess (a) the sensitivity of each of the hazard parameters in the resulting hazard maps and (b) also their relative importance in the results. To answer these, different combinations of hazard maps are developed based on individual parameters (depth, duration, and area) as well as a combined parameter (Figure 7). These figures explain how the different hazard parameters will influence the resulting hazard maps individually and combinedly. The sensitivity analysis further shows that the combined hazard map better represents the actual flood scenario for the study area than the ones prepared on the individual parameter. For example, if only depth or duration is considered, the Maksudpur is found in a high and very high hazard zone in the 2080s of RCP8.5 (Figure 7f or 7l). But if the flood maps are critically observed (Figure 6), it is evident that it (Maksudpur) is far from the Arial Khan and Padma River. So, it is usually flooded only in high floods (Figure 6f, 6l, and 6r). However, as it is a low-lying area (Supp. Figure 7), the flood water remains there for a long duration. So, depth and duration are found high there, even though the inundation area is minimal. Since only one parameter (either depth or duration) is considered, Maksudpur falls into the High Hazard zone. The inclusion of inundation area along with depth and duration represents the real flood scenario of Maksudpur. So, all three parameters seem sensitive for the hazard assessment of the Arial Khan floodplain. So, the combined hazard maps are used for the rest of the paper.

The next question is the relative importance of each of the three selected parameters in the final hazard maps. For this, the corresponding weightage factors of depth (a of Equation (9)), duration (b of Equation (9)), and area (c of Equation (9)) are tested by the trial-and-error method. Five trials are given as 1st Trial :(0.333, 0.333, 0.333), 2nd trial: (0.4, 0.3, 0.3), 3rd Trial: (0.3, 0.4, 0.3), 4th Trial: (0.3, 0.3,0.4) and 5th Trial: (0.35, 0.35, 0.25) (Table 6). No difference between the first and second trials is found. A very insignificant difference is found in the rest of the trials (marked by grey). Among the total 48 sets, three sets are found different in the 3rd and 4th Trials, and seven sets are found different in the 5th Trial (marked by grey). Since the difference is not very significant, an equal weightage of 0.333 is adopted for each hazard indicator. However, these sensitivity results might be useful for planners and policymakers to capture the future hazard characteristics of the Upazilas under a given set of percentage and weightage conditions. For example, Madaripur might be in either High, or Very High, or Low or Medium Hazard in the 2020s of RCP8.5, depending on the selection of the hazard parameter. Again, Bhanga may fall in either Medium or High Hazard zone in the 2050s of RCP 2.6 and RCP 8.5 if higher weightage is given to either depth (2nd Trial) or duration (3rd Trial). The same happens to Rajoir in the 2020s of RCP 2.6. Given higher weightage to either depth (2nd trial) or area (4th Trial), Maksudpur may fall in either Medium or High Hazard zone in the 2080s of RCP 2.6, Rajoir may fall in either Medium or High Hazard zone in 2050s of RCP 2.6 and 2020s of RCP 8.5 and Shariatpur might fall in either Medium or High range in the 2020s, 2050s of RCP 2.6 and 2020s, 2050s of RCP 8.5.

Table 5 | Upazila-wise flood inundated area (km^2) under RCP 2.6 and RCP 8.5

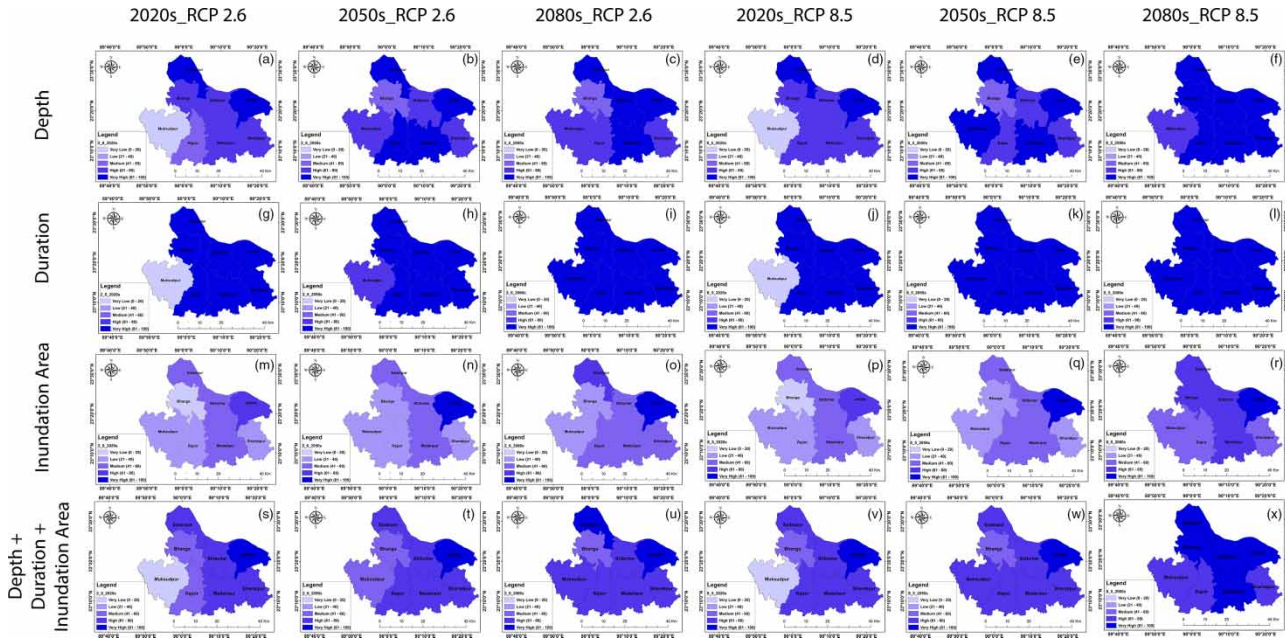| Upazila | Flood Affected Area (km^2) | | | | | |
| | RCP 2.6 | | | RCP 8.5 | | |
	2020s	2050s	2080s	2020s	2050s	2080s
Bhanga	0	2	5	0	2	100
Sadarpur	51	72	76	52	73	81
Maksudpur	0	7	17	0	7	109
Madaripur	65	94	113	70	104	131
Rajoir	24	38	55	30	48	84
Shibchar	50	64	73	50	69	94
Shariatpur	11	26	45	14	33	60
Zanjira	114	135	138	114	137	139
Total	316	437	523	330	473	798

Figure 7 | Hazard maps considering individual parameter (depth, duration, area) and combination of the three parameters.

4.5. Future flood hazard assessment

The Spatio-temporal change of hazard zones for RCP2.6 and RCP8.5 are shown in Figure 7 (s, t, u, v, w, and x). The 2020s of RCP8.5 is similar to that of RCP2.6 except for Rajoir, which falls in the high hazard zone. Maksudpur, Sadarpur, Bhanga, Madaripur, and Shibchar have become more hazardous from the 2020s to the 2080s under the RCP8.5 climate scenario. The percentage area under different hazard zones for both RCP2.6 and 8.5 are summarized in Table 8a. In the 2020s of RCP2.6, 18, 24, 47, and 11% are found in the very low, medium, high, and very high hazard zones. On the other side, during the 2020s of RCP8.5, 18, 11, 60, and 11% are found in the very low, medium, high, and very high hazard zones. In the 2020s, there is only one area under a very high hazard zone. However, it has changed to 11% in the medium, 68% in the high, and 21% in the very high hazard zone in the 2080s of RCP2.6. In the 2080s of RCP8.5, the scenario is more alarming. While no area falls in the very low, low, and medium hazard zone, 41 and 59% of the area fall under the high hazard and very high hazard zone, respectively. So, low and very low hazard zone will be diminishing at the end of the century. On the contrary, high and very high hazard zone will increase due to climate change impact.

4.6. Exposure and vulnerability assessment

The relative contribution of the normalized indicators of exposure and vulnerability for each of the Upazilas is shown in Figure 8(a)–8(c). The weightage of the selected indicators was calculated individually in SPSS statistics both for exposure and vulnerability using PCA, as shown in Table 7. The exposure and vulnerability map of the Arial Khan River floodplain is shown in Figure 9(a) and 9(b).

Figure 9(a) shows that 28, 27, 0, 21, and 24% are under Very Low, Low, Medium, High, and Very High exposure zones, respectively. It further shows that the exposure is least in Zanjira and Sadarpur. The reason behind this is the low population density, household, and cropped land in these two Upazilas (Figure 8(a)). As there are few populations and croplands in these areas, they are less exposed to floods. On the other hand, the population and cropland are high in Shibchar and Madaripur (Figure 8(a)). Hence, they are more exposed to flood hazards.

The Upazila-wise vulnerability zones are shown in Figure 9(b). The percentage areas are 11, 22, 0, 37, and 29% under Very Low, Low, Medium, High, and Very High vulnerability zones. Madaripur is found the least vulnerable among all the Upazilas due to its low disabled population, dependent population ratio, female to male ratio, and poverty rate (Figure 8(b)). Contrary, adaptive capacities such as pucca and semi-pucca houses, communication infrastructure, crop productivity, literacy, health centre, flood shelter, and growth centre are high (Figure 8(c)). Madaripur is highly developed as a district town, i.e., less flood sensitive and highly adaptive compared to other Upazilas. It is the only Upazila that has a flood forecasting and warning

Table 6 | Weightage assignment for the hazard parameters by trial-and-error method

Trials	Upazila	2020s_RCP2.6	2050s_RCP2.6	2080s_RCP2.6	2020s_RCP8.5	2050s_RCP8.5	2080s_RCP8.5
1st Trial: 0.33,0.33,0.33	Bhanga	Medium	Medium	Medium	Medium	Medium	Very High
	Sadarpur	High	High	Very High	High	High	Very High
	Muksudpur	Very Low	Medium	High	Very Low	High	High
	Madaripur	High	High	High	High	High	Very High
	Rajoir	Medium	High	High	High	High	High
	Shibchar	High	High	High	High	High	Very High
	Shariatpur	High	High	High	High	High	High
	Janjira	Very High	Very High	Very High	Very High	Very High	Very High
2nd Trial: 0.4,0.3,0.3	Bhanga	Medium	Medium	Medium	Medium	Medium	Very High
	Sadarpur	High	High	Very High	High	High	Very High
	Muksudpur	Very Low	Medium	High	Very Low	High	High
	Madaripur	High	High	High	High	High	Very High
	Rajoir	Medium	High	High	High	High	High
	Shibchar	High	High	High	High	High	Very High
	Shariatpur	High	High	High	High	High	High
	Janjira	Very High	Very High	Very High	Very High	Very High	Very High
3rd Trial: 0.3, 0.4,0.3	Bhanga	Medium	High	Medium	Medium	High	Very High
	Sadarpur	High	High	Very High	High	High	Very High
	Muksudpur	Very Low	Medium	High	Very Low	High	High
	Madaripur	High	High	High	High	High	Very High
	Rajoir	High	High	High	High	High	High
	Shibchar	High	High	High	High	High	Very High
	Shariatpur	High	High	High	High	High	High
	Janjira	Very High	Very High	Very High	Very High	Very High	Very High
4th Trial: 0.3, 0.3,0.4	Bhanga	Medium	Medium	Medium	Medium	Medium	Very High
	Sadarpur	High	High	Very High	High	High	Very High
	Muksudpur	Very Low	Medium	Medium	Very Low	High	High
	Madaripur	High	High	High	High	High	Very High
	Rajoir	Medium	Medium	High	Medium	High	High
	Shibchar	High	High	High	High	High	Very High
	Shariatpur	Medium	Medium	High	Medium	Medium	High
	Janjira	Very High	Very High	Very High	Very High	Very High	Very High
5th Trial: 0.35,0.35, 0.25	Bhanga	Medium	High	Medium	Medium	High	Very High
	Sadarpur	High	High	Very High	High	High	Very High
	Muksudpur	Very Low	Medium	High	Very Low	High	High
	Madaripur	High	High	High	High	High	Very High
	Rajoir	High	High	High	High	High	High
	Shibchar	High	High	High	High	High	Very High
	Shariatpur	High	High	High	High	High	High
	Janjira	Very High	Very High	Very High	Very High	Very High	Very High

station. Hence, Madaripur falls in the very low-vulnerable zone. Again, though Zanjira falls into the very low exposed zone, it has the highest vulnerability. Because the percentage of dependable people and the poverty rate are the highest here. At the same time, pucca and semi- pucca houses, communication infrastructure, and growth centre numbers are very low.

4.7. Future flood risk assessment

When vulnerability and exposure are combined with hazard, flood risk zones are identified across the floodplains of the Arial Khan River. Figure 10(a)–10(f) shows the spatio-temporal change of flood risk zones for each of the Upazilas of the study area under RCP2.6 and RCP8.5. The percentage of areas under different risk zones under RCP2.6 and RCP8.5 are shown in Table 8(b). In the 2020s under RCP2.6 scenarios, 55, 33, and 11% are under the very low, low, and medium risk zones. It becomes 37% in the very low-risk zone, 21% in the low-risk zone, 24% in the medium-risk zone, and 18% in the very high-risk zone in the 2080s under RCP2.6. On the other hand, it is 37, 10, 24, 11, and 18% in the very low, low, medium,

Table 7 | Weightage of exposure and vulnerability indicators from PCA

| Component		Indicator	Weightage Factor
Exposure		Population density	0.29
		No. of household	0.37
		Cropped land	0.34
Vulnerability	Sensitivity (-)	Disable population	0.1
		Dependent population ratio	0.07
		Female to male ratio	0.07
		Poverty rate	0.08
	Adaptive Capacity (+)	Pucca and Semi-pucca house	0.08
		Communication infrastructure	0.08
		Productivity of crop	0.09
		Literacy rate	0.07
		Health centre	0.08
		Flood shelter	0.07
		Growth centre	0.1
		Flood forecasting and warning system	0.1
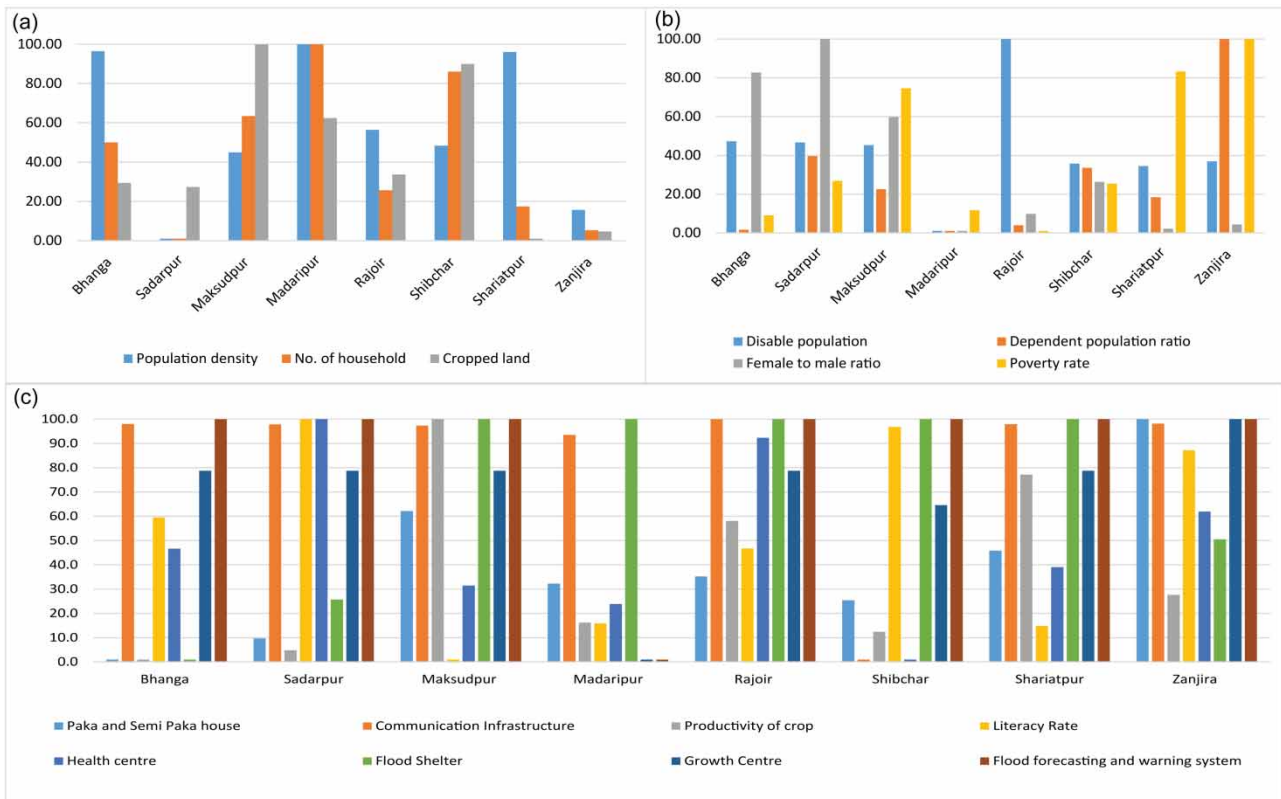
Figure 8 | Relative contribution of normalized (a) exposure indicators, (b) vulnerability indicators (+ve dependency), (c) vulnerability indicators (-ve dependency).

high, and very high hazard zone, respectively, under RCP8.5. So, it is observed that future climate change will decrease very low and low-risk zone and increase high and very high-risk zone in the 2080s under RCP8.5.

The integrated risk analysis further shows that the incorporation of vulnerability and exposure along with hazard provides a wide horizon to the overall assessment. For example, in the 2080s, Zanjira falls in the high hazard zone. However, when the associated exposure and vulnerability indices are considered, it falls in a low-risk area. Though this Upazila is profoundly affected by the flood, the exposure and vulnerability are low. Hence, overall flood risk has been decreased. Therefore, despite
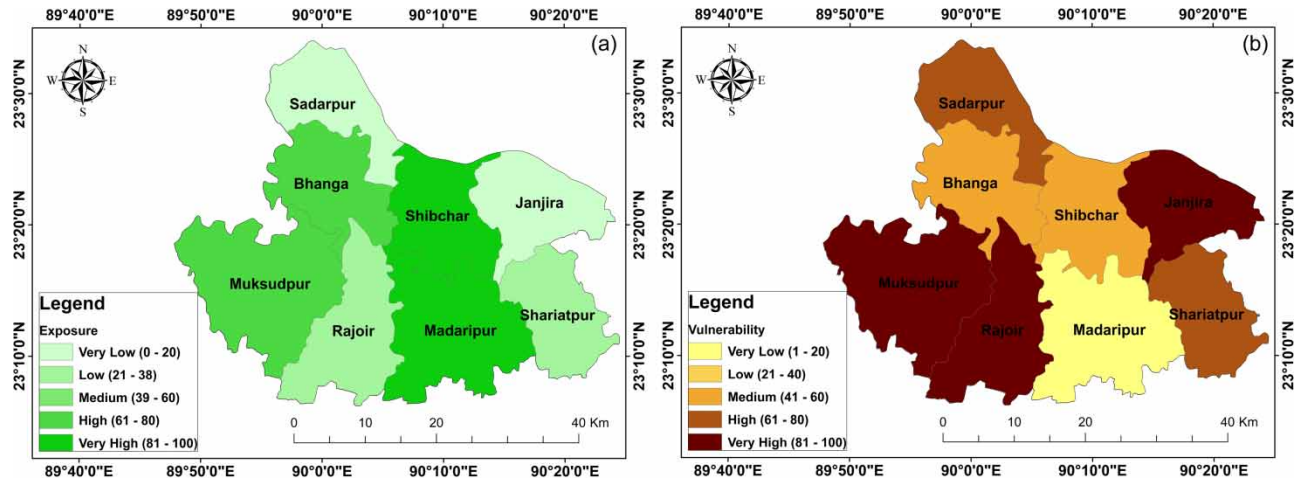
Figure 9 | Upazila-wise (a) exposure and (b) vulnerability map of the study area.
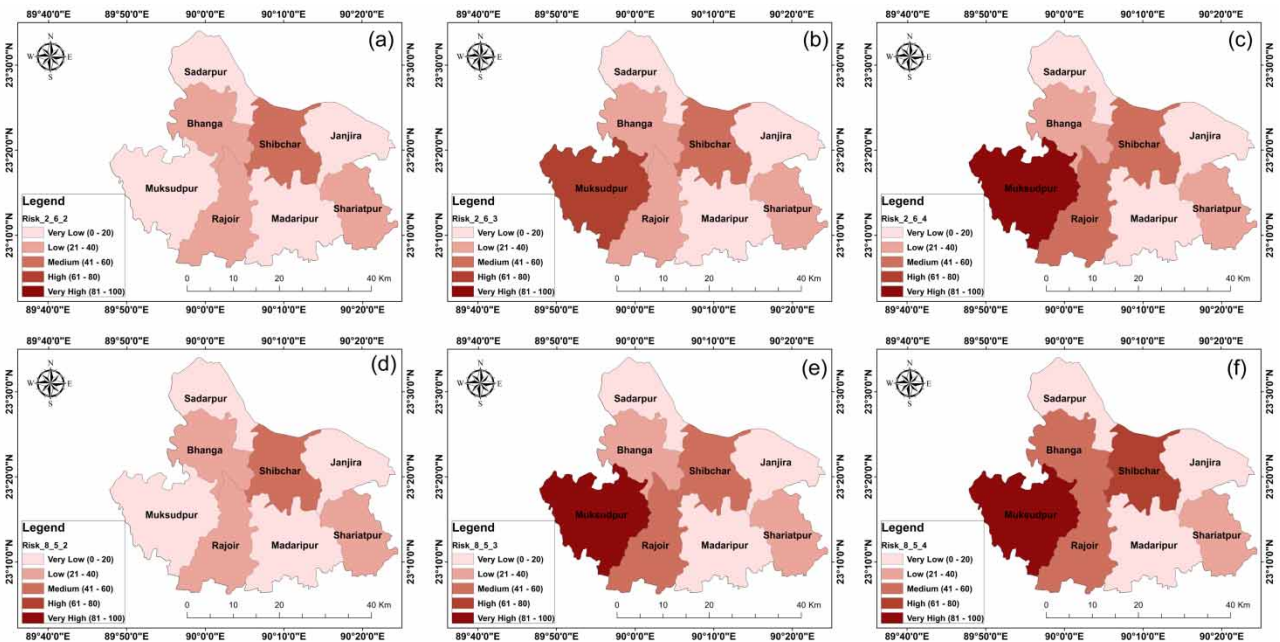

Figure 10 | Flood risk maps in (a) 2020s (b) 2050s (c) 2080s under RCP2.6 and in (d) 2020s (e) 2050s (f) 2080s under RCP8.5.

its high hazardous categorization, it becomes a very low-risk zone in the 2080s. The opposite happens for Madaripur. If only the flood hazard factor is considered, it falls in a low hazard zone. However, it falls under the very high-risk area, when vulnerability and exposure factors are considered hazard factors. Because both exposure and vulnerability factors are high for Madaripur. Likewise, the hazard maps change patterns when they are converted to risk maps.

Some medium hazard zones fall into high-risk zones due to their high exposure and vulnerability to flooding. In contrast, some high hazard zone falls into the low-risk area because of its low exposure and vulnerability. Hence, allocation of resources or flood management plans should be made based on hazard and risk analysis. For example, a high hazardous area might be protected with structural measures such as embankment, dredging, river training works, etc. On the other hand, a highly exposed site to floods might be restricted for cultivating lands and building houses or infrastructures. In such cases, allocation of resources such as pucca and semi-pucca houses, communication infrastructures, health centres, flood shelters, growth centres, flood forecasting and warning system will certainly increase the adaptive capacity of the community, but cannot eliminate its flood risk and damage.

Table 8 | Percentage of the area under different (a) hazard and (b) risk zones for RCP 2.6 and RCP 8.5

| Type | Scenario | Period | Percentage of Area | | | | |
			Very Low	Low	Medium	High	Very High
(a) Hazard	RCP 2.6	2020s	18	0	24	47	11
		2050s	0	0	29	60	11
		2080s	0	0	11	68	21
	RCP 8.5	2020s	18	0	11	60	11
		2050s	0	0	11	78	11
		2080s	0	0	0	41	59
(b) Risk	RCP 2.6	2020s	55	33	11	0	0
		2050s	37	33	11	18	0
		2080s	37	21	24	0	18
	RCP 8.5	2020s	55	33	11	0	0
		2050s	37	21	24	0	18
		2080s	37	10	24	11	18

On the other hand, a low hazardous area with a high socio-economic vulnerable community needs more pucca and semi-pucca houses, communication infrastructures, flood shelters, health centres, growth centres, flood forecasting and warning system, and employment opportunity. So, hazard-risk maps make it easier to plan which plan or strategy should be taken for a certain Upazila and that too staying within a limited budget. Thus, it is very important to consider each of the risk components, i.e., hazard, exposure, and vulnerability, and their integrated results for a sustainable flood management plan.

5. DISCUSSION

The observed flood pattern shows that since the riverine flood is caused due to water flowing over the river banks, the Upazilas (Shibchar, Bhanga, and Madaripur) along the river are found with higher flood depth, duration, and area (Figure 6). Hazard is entirely dependent on these three parameters, so the same pattern has been observed in hazard maps as well (Figure 9). Janjira and Sadarpur are found in the high hazardous category due to the flood impact of the Padma River. In brief, the Upazilas along the left reach of the Arial Khan River is found more hazard-prone at the end of the 21st century. Flood risk is associated with the hazard, exposure, and vulnerability. Hence, the risk zones do not follow the same spatial distribution/pattern as flood or hazard maps. Instead, the Upazilas on the right side (Bhanga, Maksudpur, and Rajoir) of the Arial Khan River are found more risk-prone (Figure 10). These three Upazilas are low to medium exposed to flood (Figure 9(a)). Bhanga is very high hazard-prone (Figure 7(x)), and Maksudpur and Rajoir are high flood vulnerable (Figure 9(b)). Hence, combining all three components, these are found in high risk-prone zones.

The temporal pattern of the flood maps shows consonance with the IPCC AR5 report. According to this report, CO_2 concentration, global temperature, northern sea-ice extent, sea-level rise remain almost similar from baseline to 2020s for both RCP2.6 and RCP8.5 scenario (IPCC 2014). Then the differences between the RCP2.6 and RCP8.5 scenario becomes very rapid and high after the 2050s. Similar trends are found in the current study. The difference between RCP2.6 and RCP8.5 is found minimal from the 2020 to 2050s but becomes very pronounced in the 2080s (Figure 6). Furthermore, according to IPCC AR5, the global surface temperature is likely to exceed 1.5 °C at the end of the 21st-century relatives to the base period (1850 to 1900) for all RCP scenarios except RCP2.6. It is likely to exceed 2 °C under RCP 6.0 and RCP8.5 and more likely not to exceed 2 °C under RCP 4.5. Moreover, it is also stated that warming will continue beyond 2100 under all RCP scenarios except under RCP2.6 (IPCC 2014). Hence, inundation depth, duration, and area are found much higher in RCP8.5 than RCP2.6, and they are the highest in the 2080s of RCP8.5. The results of this study harmonize with the recent flood studies conducted in the nearby countries considering RCP emission scenarios as well. Shrestha & Lohpaisankrit (2017) reported that flood depth and area would be the maximum by the end of the 21st century under the RCP8.5 projection in the Yang Basin of Thailand. The recent studies by Nishat (2017) and Rahman (2019) on the Brahmaputra and Old Brahmaputra River of Bangladesh also show a significant increase of high to very high hazard and risk zone by the end of 2100 under RCP8.5.

The present flood hazard and risk maps are compared with the hazard and risk maps of Tingsanchali & Karim (2005) that were developed focusing the whole south-west river system of Bangladesh based on stationary hydrologic data and without considering the upstream basin flow from the Ganges and Brahmaputra rivers. The previous study found higher hazard-prone areas along with the Arial Khan and Padma River for a 100-year historic flood as found in the present study by the end of the 21st century under RCP 8.5. On the other hand, a significant difference is found in the risk maps. The reasons might be – a) the current study uses the most recent Population Census 2011 while the previous study used past Population Census, b) the current study considers fifteen important vulnerability and exposure indicators and their relative weights while the previous study considered only one vulnerability input, i.e., the population density, and c) the current study computes integrated flood risk as to the product of the hazard, exposure, and vulnerability using IPCC risk framework while the previous study computed flood risk as to the product of hazard and vulnerability. Most importantly, hazard and risk maps are qualitative studies focusing on qualitative comparisons of flood threats among the considered study areas. As the areal extent between the previous study and the current study is not the same and the input parameters and approaches are significantly different, it's not possible to precisely compare the findings of these two studies. The present study is focused on the Arial Khan River and considered many important factors which were completely ignored in the past study. Hence, this study will provide more reliable flood hazard and risk results for the Arial Khan River under future climate change scenarios.

Overall, flood hazard and risk maps prepared in this study give a qualitative view of the potential flood scenarios for the eight Upazilas of the Arial Khan River. The hazard and risk maps will be useful in identifying the priority areas for allocating flood reliefs and planning a long-lasting future flood management strategy along the Arial Khan River. For example, the hazard and risk maps of the 2020s or 2050s can be incorporated into the short-term or mid-term plans. Additionally, the maps of the 2080s can be incorporated into any long-term plan, such as a 100-year plan. The recently approved 'Bangladesh Delta Plan 2100' implementation would also benefit from these flood risk maps (BDP 2017). Additionally, different hazard combinations (Depth, Duration, Area, and Depth + Duration + Area) and weightage trials (0.33,0.33,0.33; 0.4,0.3,0.3; 0.3,0.4,0.3; 0.3,0.3, 0.4; 0.35,0.35, 0.25) are also provided. So, hazard prediction that any Upazila may face in the near (the 2020s), mid (2050s), or end (2080s) future under a given set of parameters and weightage can be made. The planners and policymakers can take any of these combinations and make a tentative recommendation to decision-makers.

In this study, physics-based traditional numerical models – SWAT and HEC-RAS are used for computing the future flood hazard of the Arial Khan River floodplain using EC-Earth-HR projected climate data. Such a multi-model hydrology-hydrodynamic modelling system is an appropriate way to incorporate the climate change impact of large basins (Ganges and Brahmaputra) into a local river (Arial Khan). However, various uncertainties may find in the predictions made by the numerical models. For example, the SWAT has several parameters and model simplifications that introduce uncertainty in the basin model. Besides, generated SWAT flow is used as input for the hydrodynamic HEC-RAS models. These numerical models have been calibrated and validated with satisfactory results and demonstrated adequacy to represent the hydrologic and hydraulic behaviour of the study area. Nevertheless, applying such models for transforming regional flows into local scale flood prediction might introduce few uncertainties in the result. The major uncertainties resulting from the hydrologic models, hydraulic models, and regression models are quantified using NRMSE (Table 9). These uncertainties might impact the resulting hazard maps. However, the uncertainties are found much smaller in the flood season, proving the models' efficiency in flood hazard analysis and solidifying the acceptance of this study. Considering the total percentage, nearly 48% of uncertainty might come from the hydrologic models, 23% from the hydraulic models, and 28% from the statistical regression model. The models' uncertainties can be estimated using some advanced tools such as variance-based methods (Saltelli et al. 2008; Tate et al. 2015), Sobol's method (Saisana et al. 2005), Fourier amplitude sensitivity test (FAST) (Saltelli et al. 1999), etc. in the future study.

The d/s boundary of the flood model is defined by the sea-level-rise (SLR) of 55–82 cm for the RCP2.6 and 8.5 scenarios provided by the IPCC AR5 report (IPCC 2014) without taking the actual SLR projections at that location. According to Mondal et al. (2018), increase of peak water level is 72 cm at Chandpur station of the Meghna River for RCP 8.5, which is very close to our downstream model boundaries (Sureswar – SW95 and Madaripur – SW5). Here, the % of error is nearly (82–72) *100/82 = 12%. However, as our downstream model boundary in the Arial Khan River is a little downstream of the Chandpur, the increase of peak stage will be slightly higher than 72 cm due to SLR. Thus, comparing with Mondal et al. (2018), the % of error would be less than <10%, which can be neglected considering the uncertainties of climate model projections.

In this study, the vulnerability and exposure data are kept constant throughout the end of the century. The incorporation of Shared Socioeconomic Pathways (SSPs) could be a way to estimate future vulnerability and exposure data and thereby assess the actual risk scenarios in the future. The climate change research community recently adopted the SSPs framework to

Table 9 | Estimation of standard error using NRMSE method for each of the developed model components

Models		Model		Flood Season	
		NRMSE	% Error	NRMSE	% Error
Hydrologic Models	SWAT model (Brahmaputra)	0.33	10.76	0.27	13.64
	SWAT model (Ganges)	1.39	45.69	0.66	34.14
Statistical Model	Linear Regression model	0.56	18.20	0.56	28.59
Hydraulic Models	1D HEC-RAS model	0.12	4.07	0.12	6.39
	1D2D HEC-RAS model (1D model)	0.58	18.87	0.26	13.44
	1D2D HEC-RAS model (Flood model)	0.07	2.42	0.07	3.80

facilitate integrated analysis on future climate change, vulnerabilities, adaptation, and mitigation (O'Neill *et al.* 2014; Van Vuuren *et al.* 2014). In SSPs, population, GDP, and urbanization data are provided on a global scale. Later, the country scale, or sub-national scale, or multi-scale, or participatory scenario approach is quantified applying the global RCP–SSP–SPA scenario framework (Kebede *et al.* 2018). However, it is hard to get the future projections of each of the fifteen exposure and vulnerability indicators used in this study. Hence, SSPs are kept beyond the scope of this study. Nevertheless, it could be an exciting topic for future studies.

6. CONCLUSION

Climate change impact on potential flood hazard and risk of the Arial Khan River floodplain are evaluated incorporating the recent RCP climate scenarios and AR5 risk framework. An increasing trend in flood depth, duration, and area is observed from the early (2020s) to the end (2080s) of the century for both RCP2.6 and 8.5 scenarios. The situation is far worsening for RCP8.5, as expected. The increase in flood depth, duration, and extent must be considered while designing any hydraulic/stormwater structures or flood measures along the flood plain. The sensitivity analysis of the hazard parameters shows that the combined parameters (Depth + Duration + Area) with equal weightage (0.33,0.33,0.33) represent the flood scenario better for the study area. The Upazilas along the left reach of the Arial Khan River is found more hazard-prone, while the Upazilas on the right side of the Arial Khan River is found more risk-prone in the 2080s of RCP8.5. The Upazila-wise hazard maps reveal that the high and very high hazard zone will significantly expand in the 2080s of RCP8.5. Similarly, risk assessment shows that the very low and low-risk zone will decrease, and the high and very high-risk areas will increase by the end of the 21st century for RCP8.5. The hazard-risk maps further make it easier to plan which plan or strategy should be taken for a certain Upazila within a limited budget. Thus, it is very important to consider each of the risk components, i.e., hazard, exposure, and vulnerability, and their integrated results for a sustainable flood management plan. The results found in this study are found quite acceptable, comparing the IPCC climate studies and other relevant studies conducted in this region. Future studies can be extended by introducing the RCP–SSP–SPA scenario framework.

The flood hazard and risk maps provide useful information to policymakers regarding emergency preparedness and relief operations for high-risk and very high-risk zones in future flood events of Arial Khan. Besides, compared to the wide range of research conducted in other flood-prone countries, research work in Bangladesh on future flood situations considering transboundary basin flow and recent climate change scenarios is very limited. This study presents a methodology to incorporate the climate impact of large transboundary basins to a small local river using combined hydrological, hydrodynamic, and statistical models and how to check their regional adequacy for the study area. Hence, it will be helpful for other researchers to work on the future flood scenarios of Bangladesh considering climate change impact.

DATA AVAILABILITY STATEMENT

Data cannot be made publicly available; readers should contact the corresponding author for details.

REFERENCES

Abbaspour, K. C., Yang, J., Maximov, I., Siber, R., Bogner, K., Mieleitner, J., Zobrist, J. & Srinivasan, R. 2007 Modeling hydrology and water quality in the pre-alpine/alpine Thur watershed using SWAT. *Journal of hydrology* **333** (2–4), 413–430. https://doi.org/10.1016/j.jhydrol.2006.09.014.

Ahmadisharaf, E., Kalyanapu, A. J. & Chung, E. S. 2017 Sustainability-based flood hazard mapping of the Swannanoa River watershed. *Sustainability* **9** (10), 1735.

Ahsan, M. N. & Warner, J. 2014 The socio-economic vulnerability index: a pragmatic approach for assessing climate change led risks–A case study in the south-western coastal Bangladesh. *International Journal of Disaster Risk Reduction* **8**, 32–49.

Akter, J., Sarker, M. H. & Haque, P. 2013 Morphological processes and effective river erosion management: a case study of the Arial Khan River in Bangladesh. In: *Proc. of the 4th International Conference on Water and Flood Management*, Dhaka, Bangladesh.

Ali, M. H., Bhattacharya, B., Islam, A. K. M. S., Islam, G. M. T., Hossain, M. S. & Khan, A. S. 2019 Challenges for flood risk management in flood-prone Sirajganj region of Bangladesh. *Journal of Flood Risk Management* **12** (1), e12450.

Allen, S. K., Linsbauer, A., Randhawa, S. S., Huggel, C., Rana, P. & Kumari, A. 2016 Glacial lake outburst flood risk in Himachal Pradesh, India: an integrative and anticipatory approach considering current and future threats. *Natural Hazards* **84** (3), 1741–1763.

Amiri, M. A. & Mesgari, M. S. 2017 Modeling the spatial and temporal variability of precipitation in northwest Iran. *Atmosphere* **8** (12), 254.

Amiri, M. A. & Mesgari, M. S. 2019 Spatial variability analysis of precipitation and its concentration in Chaharmahal and Bakhtiari province, Iran. *Theoretical and Applied Climatology* **137** (3), 2905–2914.

Amiri, M. A., Mesgari, M. S. & Conoscenti, C. 2017 Detection of homogeneous precipitation regions at seasonal and annual time scales, northwest Iran. *Journal of Water and Climate Change* **8** (4), 701.

Bangladesh Bureau of Statistics (BBS) 2020 *Bangladesh Bureau of Statistics (BBS)*. Available from: http://www.bbs.gov.bd/ (accessed 1 March 2020).

BDP 2017 *Bangladesh Delta Plan 2100. General Economics Division, Bangladesh Planning Commission. (2017)*. Government of the People's Republic of Bangladesh.

Beniston, M., Stephenson, D. B., Christensen, O. B., Ferro, C. A., Frei, C., Goyette, S., Halsnaes, K., Holt, T., Jylhä, K., Koffi, B. & Palutikof, J. 2007 Future extreme events in European climate: an exploration of regional climate model projections. *Climatic Change* **81** (1), 71–95.

Betancur-Pérez, G., Toro-Botero, F. M. & Gómez-Giraldo, A. 2016 Methodology for hydrodynamic model selection: case study: spatial variability of the thermal structure in the Riogrande II tropical reservoir, Colombia. *Dyna* **83** (198), 154–164.

Bonsal, B. R., Zhang, X., Vincent, L. A. & Hogg, W. D. 2001 Characteristics of daily and extreme temperatures over Canada. *Journal of Climate* **14** (9), 1959–1976.

Braun, M. R., Altan, H. & Beck, S. B. M. 2014 Using regression analysis to predict the future energy consumption of a supermarket in the UK. *Applied Energy* **130**, 305–313.

Brouwer, R., Akter, S., Brander, L. & Haque, E. 2007 Socio-economic vulnerability and adaptation to environmental risk: a case study of climate change and flooding in Bangladesh. *Risk Analysis: An International Journal* **27** (2), 313–326.

Brunner, G. W. 2016 HEC-RAS River Analysis System: Hydraulic Reference Manual. U.S. Army Corps of Engineers, Institute for Water Resources, Hydrologic Engineering Center, 609 Second Street, Davis, CA 95616.

Brunner, G. W., Piper, S. S., Jensen, M. R. & Chacon, B. 2015 Combined 1D and 2D hydraulic modeling within HEC-RAS. In: *World Environmental and Water Resources Congress 2015*, pp. 1432–1443.

Brunner, G. W. 2016 HEC-RAS river analysis system 2D modeling user's manual. US Army Corps of Engineers–Hydrologic Engineering Center, Davis, CA, pp. 1–171.

BWDB 2011 *Bangladesh er Nod-Nodi*. Bangladesh Water Development Board, Dhaka, Bangladesh.

Costabile, P., Costanzo, C., Ferraro, D., Macchione, F. & Petaccia, G. 2020 Performances of the new HEC-RAS version 5 for 2-D hydrodynamic-based rainfall-runoff simulations at basin scale: comparison with a state-of-the art model. *Water* **12** (9), 2326.

Cutter, S. L., Boruff, B. J. & Lynn Shirley, W. 2003 *Social Vulnerability to Environmental Hazards Social Science Quarterly*.

Dankers, R. & Feyen, L. 2008 Climate change impact on flood hazard in Europe: an assessment based on high-resolution climate simulations. *Journal of Geophysical Research: Atmospheres* **113** (D19), 1–17.

Das, P., Noor, L., Islam, F. & Khan, S. 2018 Flood Inundation Mapping on Surma-Kusiyara Floodplain Using HEC-RAS 1D/2D Couple Model. In: *E-proceedings of the 8th International Symposium on Environmental Hydraulics (ISEH 2018)*, June 4–7, 2018. University of Notre Dame, Indiana, USA.

Flood Forecasting and Warning Center (FFWC) 2018 *FFWC Annual Flood Report 2018*. FFWC, Bangladesh Water Development Board (BWDB). Available from: http://www.ffwc.gov.bd/images/annual17.pdf (accessed 31 March December 2020).

Fossati, M. & Piedra-Cueva, I. 2013 A 3D hydrodynamic numerical model of the Río de la Plata and Montevideo's coastal zone. *Applied Mathematical Modeling* **37** (3), 1310–1332.

Gbetibouo, G. A., Ringler, C. & Hassan, R. 2010 Vulnerability of the South African farming sector to climate change and variability: an indicator approach. In: *Natural Resources Forum*, Vol. 34(3), pp. 175–187. doi:10.1111/j.1477-8947.2010.01302.x.

Gisen, D. C., Weichert, R. B. & Nestler, J. M. 2017 Optimizing attraction flow for upstream fish passage at a hydropower dam employing 3D Detached-Eddy Simulation. *Ecological Engineering* **100**, 344–353.

Gusain, A., Mohanty, M. P., Ghosh, S., Chatterjee, C. & Karmakar, S. 2020 Capturing transformation of flood hazard over a large River Basin under changing climate using a top-down approach. *Science of the Total Environment* **726**, 138600.

Hazeleger, W., Wang, X., Severijns, C., Ştefănescu, S., Bintanja, R., Sterl, A., Wyser, K., Semmler, T., Yang, S., Van den Hurk, B. & Van Noije, T. 2011 EC-earth V2.2: description and validation of a new seamless earth system prediction model. *Climate Dynamics* **39**, 2611–2629. doi:10.1007/s00382-011-1228-5.

International Panel on Climate Change (IPCC) 2013 IPCC, 2013: Summary for Policymakers. In: *Climate Change 2013: The Physical Science Basis. Contribution of Working Group I to the Fifth Assessment Report of the Intergovernmental Panel on Climate Change* (Stocker, T. F., Qin, D., Plattner, G.-K., Tignor, M., Allen, S. K., Boschung, J., Nauels, A., Xia, Y., Bex, V. & Midgley, P. M., eds.). Cambridge University Press, Cambridge, United Kingdom & New York, NY, USA.

International Panel on Climate Change (IPCC) 2014 IPCC, 2014: Climate Change 2014: Synthesis Report. In: *Contribution of Working Groups I, II and III to the Fifth Assessment Report of the Intergovernmental Panel on Climate Change* (Core Writing Team, Pachauri, R. K. & Meyer, L. A., eds.). IPCC, Geneva, Switzerland, p. 151.

International Sava River Basin Commission (ISRBC) 2014 *Preliminary Flood Risk Assessment in the Sava River Basin*. Available from: http://www.savacommission.org/dms/docs/dokumenti/documents_publications/publications/other_publications/pfra/preliminary_flood_risk_assessment_in_the_sava_river_basin_20140701.pdf.

Jahan, M. 2018 *Multi-Scale Assessment of Risks to Environmental Hazards in Coast Area of Bangladesh*. M.Sc. Thesis, Institute of Water and Flood Management, BUET, Dhaka -1000.

Kabir, R., Sakib, M., Jahan, M., Haque, A. & Rahman, M. 2017 Socio-Economic Vulnerability Assessment Due to Storm Surge Hazard in Bangladesh Coast. In: *6th International Conference on Water and Flood Management (ICWFM 2017)*, March 4–6, 2017, Dhaka, Bangladesh, pp. 277–284.

Kebede, A. S., Nicholls, R. J., Allan, A., Arto, I., Cazcarro, I., Fernandes, J. A., Hill, C. T., Hutton, C. W., Kay, S., Lázár, A. N. & Macadam, I. 2018 Applying the global RCP–SSP–SPA scenario framework at sub-national scale: a multi-scale and participatory scenario approach. *Science of the Total Environment* **635**, 659–672.

Koutroulis, A. G., Grillakis, M. G., Tsanis, I. K. & Papadimitriou, L. 2016 Evaluation of precipitation and temperature simulation performance of the CMIP3 and CMIP5 historical experiments. *Climate Dynamics* **47** (5), 1881–1898.

Koutroulis, A. G., Papadimitriou, L. V., Grillakis, M. G., Tsanis, I. K., Wyser, K., Caesar, J. & Betts, R. A. 2018 Simulating hydrological impacts under climate change: implications from methodological differences of a Pan European Assessment. *Water* **10** (10), 1331.

Lappas, I. & Kallioras, A. 2019 Flood susceptibility assessment through GIS-based multi-criteria approach and analytical hierarchy process (AHP) in a river basin in central Greece. *Parameters (Malczewski, 1999)* **6** (3), 738–751.

Larson, M., Bellanca, R., Jönsson, L., Chen, C. & Shi, P. 2005 A model of the 3D circulation, salinity distribution, and transport pattern in the Pearl River Estuary, China. *Journal of Coastal Research* **21** (5 (215)), 896–908.

Mamun, M. Y. 2008 *A Study On Offtake Morphology And Conveyance Characteristics Of Arial Khan River*. Post graduate dissertation, Bangladesh University of Engineering & Technology, Dhaka, Bangladesh. Available from: http://lib.buet.ac.bd:8080/xmlui/handle/123456789/308 (accessed 8 March 2020).

Milly, P. C. D., Betancourt, J., Falkenmark, M., Hirsch, R. M., Kundzewicz, Z. W., Lettenmaier, D. P. & Stouffer, R. J. 2008 Stationarity is dead: whither water management? *Earth* **4**, 20.

Mirza, M. M. Q. 2002 Global warming and changes in the probability of occurrence of floods in Bangladesh and implications. *Global Environmental Change* **12** (2), 127–138.

Mirza, M., Warrick, R. & Ericksen, N. 2003 The implications of climate change on floods of the Ganges, Brahmaputra and Meghna rivers in Bangladesh. *Climatic Change* **57** (3), 287–318.

Mohammed, K., Islam, A. S., Islam, G. T., Alfieri, L., Bala, S. K. & Khan, M. J. U. 2017 Extreme flows and water availability of the Brahmaputra River under 1.5 and 2 C global warming scenarios. *Climatic Change* **145** (1–2), 159–175.

Mohammed, K., Islam, A. S., Islam, G. T., Alfieri, L., Khan, M. J. U., Bala, S. K. & Das, M. K. 2018 Future floods in Bangladesh under 1.5° C, 2° C, and 4° C global warming scenarios. *Journal of Hydrologic Engineering* **23** (12), 04018050.

Mondal, M. S., Islam, A. S., Haque, A., Islam, A., Biswas, S. & Mohammed, K. 2018 Assessing high-end climate change impacts on floods in major rivers of Bangladesh using multi-model simulations. *Global Science and Technology Journal, Australia* **6** (2), 1–14.

Moriasi, D. N., Arnold, J. G., Van Liew, M. W., Bingner, R. L., Harmel, R. D. & Veith, T. L. 2007 Model evaluation guidelines for systematic quantification of accuracy in watershed simulations. *Transactions of the ASABE* **50** (3), 885–900.

Nagata, N., Hosoda, T., Nakato, T. & Muramoto, Y. 2005 Three-dimensional numerical model for flow and bed deformation around river hydraulic structures. *Journal of Hydraulic Engineering* **131** (12), 1074–1087.

Nicholas, A. R. & McLelland, S. J. 2004 Computational fluid dynamics modeling of three-dimensional processes on natural river floodplains. *Journal of Hydraulic Research* **42** (2), 131–143.

Nishat, U. 2017 *Flood Inundation Mapping of Jamuna River Floodplain Using HEC-RAS 2D Model*. B.Sc. Thesis, Department of Water Resources Engineering, Bangladesh University of Engineering & Technology, Dhaka-1000.

O'Neill, B. C., Kriegler, E., Riahi, K., Ebi, K. L., Hallegatte, S., Carter, T. R., Mathur, R. & van Vuuren, D. P. 2014 A new scenario framework for climate change research: the concept of shared socio-economic pathways. *Climatic Change* **122** (3), 387–400.

Patel, D. P., Ramirez, J. A., Srivastava, P. K., Bray, M. & Han, D. 2017 Assessment of flood inundation mapping of Surat city by coupled 1D/2D hydrodynamic modeling: a case application of the new HEC-RAS 5. *Natural Hazards* **89** (1), 93–130.

Pendergrass, A. G., Knutti, R., Lehner, F., Deser, C. & Sanderson, B. M. 2017 Precipitation variability increases in a warmer climate. *Scientific Reports* **7** (1), 1–9.

Quiroga, V. M., Kure, S., Udo, K. & Mano, A. 2016 Application of 2D numerical simulation for the analysis of the February 2014 Bolivian Amazonia flood: application of the new HEC-RAS version 5. *Ribagua* **3** (1), 25–33.

Rahman, A. 2019 *Study on Monsoon Flood Hazard and Vulnerability Assessment of Old-Brahmaputra River Floodplain Under Climate Change Scenario*. Post graduate dissertation, Bangladesh University of Engineering & Technology, Dhaka, Bangladesh.

Rajib, A., Liu, Z., Merwade, V., Tavakoly, A. A. & Follum, M. L. 2020 Towards a large-scale locally relevant flood inundation modeling framework using SWAT and LISFLOOD-FP. *Journal of Hydrology* **581**, 124406.

Rangari, V. A., Umamahesh, N. V. & Bhatt, C. M. 2019 Assessment of inundation risk in urban floods using HEC RAS 2D. *Modeling Earth Systems and Environment* **5** (4), 1839–1851.

Saisana, M., Saltelli, A. & Tarantola, S. 2005 Uncertainty and sensitivity analysis techniques as tools for the quality assessment of composite indicators. *Journal of the Royal Statistical Society: Series A (Statistics in Society)* **168** (2), 307–323.

Saltelli, A., Tarantola, S. & Chan, K. 1999 A quantitative model-independent method for global sensitivity analysis of model output. *Technometrics* **41**, 39–56.

Saltelli, A., Ratto, M., Andres, T., Campolongo, F., Cariboni, J., Gatelli, D., Saisana, M. & Tarantola, S. 2008 *Global Sensitivity Analysis: The Primer*. Wiley, West Sussex, UK.

Sarker, M. N. I., Wu, M., Alam, G. M. & Shouse, R. C. 2019 Livelihood vulnerability of riverine-island dwellers in the face of natural disasters in Bangladesh. *Sustainability* **11** (6), 1623.

Shaw, R., Mallick, F. & Islam, A. 2013 *Disaster Risk Reduction Approaches in Bangladesh*, Vol. 103. Springer, New York, NY.

Shrestha, S. & Lohpaisankrit, W. 2017 Flood hazard assessment under climate change scenarios in the Yang River Basin, Thailand. *International Journal of Sustainable Built Environment* **6** (2), 285–298.

Solaymani, H. R. & Gosain, A. K. 2015 Assessment of climate change impacts in a semi-arid watershed in Iran using regional climate models. *Journal of Water and Climate Change* **6** (1), 161–180.

Stamou, A. I., Mitsopoulos, G., Rutschmann, P. & Bui, M. D. 2018 Verification of a 3D CFD model for vertical slot fish-passes. *Environmental Fluid Mechanics* **18**, 1435–1461. https://doi.org/10.1007/s10652-018-9602-z.

Sutter, V. B. 2019 2D urban flood modeling using a numerical model of Delft3D flexible mesh: A case study in downtown of Shanghai city, China.

Tate, E., Muñoz, C. & Suchan, J. 2015 Uncertainty and sensitivity analysis of the HAZUS-MH flood model. *Natural Hazards Review* **16** (3), 04014030.

Tingsanchali, T. & Karim, M. F. 2005 Flood hazard and risk analysis in the southwest region of Bangladesh. *Hydrological Processes: An International Journal* **19** (10), 2055–2069.

Tu, V. T. & Tingsanchali, T. 2010 Flood hazard and risk assessment of Hoang Long River basin, Vietnam. In: *Proceeding of International MIKE by DHI Conference*.

Uddin, M. N., Islam, A. S., Bala, S. K., Islam, G. T., Adhikary, S., Saha, D., Haque, S., Fahad, M. G. R. & Akter, R. 2019 Mapping of climate vulnerability of the coastal region of Bangladesh using principal component analysis. *Applied Geography* **102**, 47–57.

UN 1991 *Mitigating Natural Disasters: Phenomena, Effects and Options: A Manual for Policy Makers and Planners*. UN Publications, New York.

Van Vuuren, D. P., Kriegler, E., O'Neill, B. C., Ebi, K. L., Riahi, K., Carter, T. R., Edmonds, J., Hallegatte, S., Kram, T., Mathur, R. & Winkler, H. 2014 A new scenario framework for climate change research: scenario matrix architecture. *Climatic Change* **122** (3), 373–386.

Vozinaki, A. E. K., Morianou, G. G., Alexakis, D. D. & Tsanis, I. K. 2017 Comparing 1D and combined 1D/2D hydraulic simulations using high-resolution topographic data: a case study of the Koiliaris basin, Greece. *Hydrological Sciences Journal* **62** (4), 642–656.

Winkley, B. R., Lesleighter, E. J. & Cooney, J. R. 1994 Instability problems of the Arial Khan River, Bangladesh. In: *The Variability of Large Alluvial Rivers* (S. A. Schumm & B. R. Winkley, eds.), ASCE, New York, pp. 269–284.

Yang, X. 2007 *3D Numerical Modelling of the Turbulent Flow in Hydraulic Structures*. Doctoral dissertation, University of Illinois at Urbana-Champaign, USA.

Younus, M. A. F. 2017 An assessment of vulnerability and adaptation to cyclones through impact assessment guidelines: a bottom-up case study from Bangladesh coast. *Natural Hazards* **89** (3), 1437–1459.

Zhang, L., Wu, P., Zhou, T., Roberts, M. J. & Schiemann, R. 2016 Added value of high resolution models in simulating global precipitation characteristics. *Atmospheric Science Letters* **17**, 646–657.

Zhong, J., Huang, T. S. & Adrian, R. J. 1998 Extracting 3D vortices in turbulent fluid flow. *IEEE Transactions on Pattern Analysis and Machine Intelligence* **20** (2), 193–199.